Full title: Mealtime alters daily rhythm in nuclear O-GlcNAcome to regulate hepatic gene expression

Short title: Nuclear O-GlcNAcome regulates rhythmic transcription

Xianhui Liu[1,2]†, Yao D Cai[1]†, Aron Judd P. Mendiola[3], Xuehan Xu[1], Yige Luo[4], Haiyan Zheng[5], Caifeng Zhao[5], Ching-Hsuan Chen[1], Yang K. Xiang[2], and Joanna Chiu[1]*

[1]Department of Entomology and Nematology, University of California, Davis, CA, USA.
[2]Department of Pharmacology, University of California, Davis, CA, USA.
[3]Department of Medical Microbiology and Immunology, University of California, Davis, CA, USA.
[4]Department of Evolution and Ecology, University of California, Davis, CA, USA.
[5]Biological Mass Spectrometry Facility, Robert Wood Johnson Medical School and Rutgers, the State University of New Jersey, Piscataway, USA.
†These authors contributed equally to this work.

*Author for correspondence: Joanna C. Chiu (E-mail: jcchiu@ucdavis.edu)

Keywords: O-GlcNAcome, Phosphoproteome, feeding and fasting cycle, transcriptomic rhythm, mouse liver, post-translational modification

Abstract

The liver circadian clock and hepatic transcriptome are highly responsive to metabolic signals generated from feeding-fasting rhythm. Previous studies have identified a number of nutrient-sensitive signaling pathways that could interpret metabolic input to regulate rhythmic hepatic biology. Here, we investigated the role of O-GlcNAcylation, a nutrient-sensitive post-translational modification (PTM) in mediating metabolic regulation of rhythmic biology in the liver. We observed daily oscillation of global nuclear protein O-GlcNAcylation in the liver of mice subjected to natural nighttime-restricted feeding (NRF). O-GlcNAcomic analysis revealed that 11.54% of 719 O-GlcNAcylated proteins are rhythmically O-GlcNAcylated over a 24-hour day-night cycle. Proteins involved in gene expression were enriched among rhythmically O-GlcNAcylated nuclear proteins, suggesting rhythmic O-GlcNAcylation may directly shape the daily rhythmicity of the hepatic transcriptome. Furthermore, we showed that rhythmic O-GlcNAcylation can also indirectly modulate the hepatic transcriptome by interacting with phosphorylation. Specifically, several proteins harboring O-GlcNAcylation-phosphorylation interplay motif exhibit rhythmic O-GlcNAcylation and phosphorylation. We propose that O-GlcNAcylation may occur at a phospho-degron of a key circadian transcriptional activator, circadian locomotor output cycles kaput (CLOCK), thus regulating its stability and transcriptional output. Finally, we report that unnatural day time-restricted feeding (DRF) dampens O-GlcNAcylation rhythm, suggesting the disruption in liver transcriptomic rhythm previously observed in DRF condition could be mediated by dysregulation of daily protein O-GlcNAcylation rhythm. In summary, our results provide new mechanistic insights into metabolic regulation of daily hepatic transcriptomic rhythm via interplay between O-GlcNAcylation and phosphorylation and shed light on the deleterious effects of improper mealtimes.

Introduction

Circadian clocks are cell-autonomous, endogenous molecular timers that integrate environmental time cues and metabolic signals, enabling organisms to adapt to 24-hour environmental changes by exhibiting time-of-day specific physiology and behavior, such as sleep-wake cycles, feeding-fasting cycles, and metabolism [1,2]. Clock disruption is associated with a

wide range of diseases, including cancer, diabetes, and heart disease [3–6]. At the molecular level, mammalian circadian clocks are composed of interlocked transcriptional-translational feedback loops. At the core loop, brain and muscle Arnt-like protein-1 (BMAL1) and circadian locomotor output cycles kaput (CLOCK) form heterodimers and activate the expression of a repertoire of genes [7]. Among these clock-regulated genes are core clock genes that encode PERIOD (PER1, PER2 and PER3) and CRYPTOCHROME (CRY1 and CRY2) proteins, which form repressor complexes to inhibit the activity of BMAL1 and CLOCK [7]. As PER and CRY proteins degrade, transcriptional repression is relieved to initiate the next circadian transcriptional cycle. This cell-autonomous molecular clock was first characterized in the suprachiasmatic nuclei (SCN) of the hypothalamus in mammalian brain; the SCN receive light/dark signals to regulate the pace of molecular clocks [8–10]. Follow-up investigations have established that almost all peripheral tissues harbor molecular clocks, and metabolic signals from daily feeding activity appear to be more potent than light as time cues in peripheral tissues [10–13].

Among all the peripheral organs that are synchronized by feeding-fasting cycles, the liver is one of the most nutrient-sensitive [11,13–15]. Feeding nocturnal mice during daytime can reverse the phase of clock gene expression in liver within a few days [14,15]. Indeed, many studies revealed the importance of metabolic regulation of the molecular clock [16]. Adenosine-monophosphate-activated protein kinase (AMPK), a nutrient sensor, phosphorylates and destabilizes CRY1 [17]. NAD^+ is essential for the activity of Poly [ADP-ribose] polymerase 1 (PARP1), which poly(ADP-ribosyl)ates CLOCK and reduces DNA-binding of CLOCK-BMAL1 complex [18]. Despite 10-20% of the rhythmic hepatic transcriptome is driven by liver intrinsic clocks [12,19], timing of food intake has actually been shown to be the dominant driver for rhythmic liver transcriptome. 70-80% of the oscillating liver transcripts lost their rhythmicity when rhythmic feeding is disrupted in mice by fasting paradigms [20] or arrhythmic feeding [21]. Moreover, in mice with ablated clocks, time-restricted feeding can partially restore rhythmic liver transcriptome [19,20,22]. Despite that several nutrient-sensitive pathways, such as those involving CREB, AKT, mTOR, and ERK1/2, have been identified to modulate food-driven rhythmic transcripts [20,21], our understanding on the molecular mechanisms by which nutrient input regulate genome-wide rhythmic gene expression is far from complete.

O-linked-N-acetylglucosaminylation (O-GlcNAcylation) is a nutrient-sensitive post-translational modification (PTM) that modifies thousands of proteins and regulates nearly all

aspects of cellular physiology, such as transcription, translation, cell signaling, immune response, and cell cycle [23–26]. O-GlcNAcylation is nutrient-sensitive given the substrate for O-GlcNAcylation, UDP-GlcNAc, is produced from the hexosamine biosynthetic pathway (HBP), which integrates glucose, amino acid, lipid and nucleotide metabolism [23–25]. Indeed, nutrient manipulation in cell media has been shown to alter cellular UDP-GlcNAc level and O-GlcNAcylation in several mammalian cell lines [27,28]. More importantly, Durgan et al. [29] and our previous study [30] showed that O-GlcNAcylation exhibits daily rhythmicity in mouse heart and *Drosophila* tissues respectively, with the peak phase of O-GlcNAcylation rhythm closely aligned with timing of food intake. A large body of work have previously demonstrated the role of O-GlcNAcylation in regulating gene expression [23–25,31]. In the molecular clock, O-GlcNAcylation regulates the stability of transcription factors BMAL1 and CLOCK in a time-of-day manner [32]. Beyond the molecular clock, O-GlcNAcylation regulates gene expression by modifying the function of other gene-specific transcription factors [33–36], general transcriptional machineries [31,37–40], regulators of DNA methylation [41–44], chromatin remodelers [45–49], and components of RNA spliceosome [50–52]. Therefore, we hypothesize that the hepatic nuclear proteome, especially proteins involved in orchestrating gene expression, could be rhythmically modified and regulated by O-GlcNAcylation.

In addition to directly modifying substrate proteins, O-GlcNAcylation also regulates protein functions by interacting with phosphorylation. O-GlcNAcylation and phosphorylation (G-P) can target the same serine/threonine residues on substrate proteins [23,27,53]. For example, in the molecular clock, competition of O-GlcNAcylation and phosphorylation at serine 662 (S662) residue of PER2 modulates transcriptional repressor activity of PER2 [54]. O-GlcNAcylation of histone H3 inhibits its mitosis-specific phosphorylation at S10, S28, and T32 to deter entry into mitosis [47]. 5%-60% phosphoproteins have been shown to exhibit rhythmic phosphorylation over a 24-hour period in liver tissue, and regulates many aspects of liver physiology, including gene expression, metabolism, cell signaling, apoptosis, and autophagy [55–58]. Since there is extensive interplay between O-GlcNAcylation and phosphorylation, it is possible that O-GlcNAcylation indirectly regulates rhythmic liver physiology through modulating daily phosphoproteome.

In this study, we showed that hepatic nuclear proteins exhibit robust daily oscillation of O-GlcNAcylation. We then performed O-GlcNAc chemoenzymatic labeling in combination with mass spectrometry proteomics to identify O-GlcNAcylated nuclear proteins in liver and observed

that proteins involved in transcriptional regulation were enriched in rhythmically O-GlcNAcylated proteins. To investigate proteome-wide G-P crosstalk, we performed parallel TMT-phosphoproteomic analysis using the same liver samples. Potential rhythmic G-P crosstalks were identified by G-P interplay motif analysis and exemplified by CLOCK and retinoblastoma-like protein 2 (RBL2). To infer the direct and indirect roles of rhythmic O-GlcNAcome in regulating hepatic transcriptome, we conducted multi-omics analysis to evaluate correlation between daily rhythms of O-GlcNAcylation and G-P interactive phosphorylation on transcription factors and gene expression rhythms of their targets. Finally, to determine if altering timing of food intake impacts daily O-GlcNAcylation rhythm, we fed mice at unnatural day feeding time and observed dampened O-GlcNAcylation rhythm of liver nuclear proteins. Our results suggest that nutrient-sensitive O-GlcNAcylation could mediate the metabolic regulation of daily hepatic transcriptome and liver physiology by modifying proteins at the post-translational level.

Results

Hepatic nuclear protein O-GlcNAcylation exhibits robust daily oscillation

We have previously reported that protein O-GlcNAcylation, a highly nutrient-sensitive PTM, exhibits daily rhythmicity in *Drosophila* tissues, and this rhythm is altered when we modified the timing of food intake [30]. Given the mammalian liver is a highly metabolically responsive tissue [11,13–15], we hypothesize that protein O-GlcNAcylation could exhibit daily rhythmicity in the liver and contribute to the regulation of daily rhythms in liver physiology. Liver samples from C57BL/6 male mice were collected every 4 hours over a 24-hour period (12h:12h light-dark (LD)). Since restricting timing of food intake to natural feeding window in animals has been shown to enhance daily O-GlcNAcylation rhythm [30], we subjected mice to natural night time-restricted feeding (NRF). To measure O-GlcNAcylation level, the O-GlcNAc moieties on nuclear protein were biotinylated using GalT1-dependent chemoenzymatic labeling and detected using streptavidin-HRP as previously described [30,59]. We only analyzed nuclear fractions, as our primary goal for this study was to investigate nutrient-sensitive PTM mechanisms that regulate the hepatic transcriptome. We observed that a group of nuclear proteins, ranging from 50KD to 250KD, are O-GlcNAcylated (Fig 1A) and total nuclear proteins exhibit rhythmic O-GlcNAcylation over a day-night cycle, as determined by Rhythmic Analysis Incorporating Nonparametric (RAIN) [60]. Nuclear protein O-GlcNAcylation peaks at zeitgeber time (ZT) 20

(Calculated by RAIN), which is eight hours after the beginning of feeding period (Fig 1A and B). To confirm that the detected signals were indeed O-GlcNAcylated proteins, unlabeled samples were processed in parallel, where GalT1 labeling enzyme is absent. As compared to labeled samples (Lane 3-4), almost no signal was detected in the unlabeled samples (Lane 1-2), indicating the labeled signals are specific for O-GlcNAcylated proteins (Fig S1).

It is possible that feeding-fasting cycles contribute to daily rhythmicity in protein O-GlcNAcylation by rhythmically supplying UDP-GlcNAc as substrate via hexosamine biosynthetic pathway (HBP). To investigate this possibility, we performed targeted metabolomics on HBP metabolites from the same mouse livers used in the analysis of O-GlcNAcylation shown in Fig 1A. We were able to detect UDP-GlcNAc, the immediate substrate of O-GlcNAcylation, despite many of the metabolites in HBP were not detected using our current method (S1 File). Similar to what we observed in flies [30], UDP-GlcNAc exhibited daily rhythm in mouse liver, with its peak preceding daily protein O-GlcNAcylation (UDP-GlcNAc: ZT12; O-GlcNAcylation: ZT20, RAIN). Furthermore, the timing of food intake occurred earlier than the rise of UDP-GlcNAc level (feeding: ZT12-24; UDP-GlcNAc: ZT 3-7) (Fig 1C). Our data suggest that feeding-fasting cycles could drive the oscillation of UDP-GlcNAc, which results in the oscillation of protein O-GlcNAcylation.

Daily O-GlcNAcomics identifies rhythmically O-GlcNAcylated nuclear proteins

O-GlcNAcylation modifies thousands of proteins involved in many fundamental cellular processes [23–25,31]. As O-GlcNAcylation is shown to be rhythmic in liver nuclei, we hypothesize that O-GlcNAcylation regulates rhythmic liver function by modifying nuclear proteins in a time-of-day manner. To test our hypothesis, we performed daily O-GlcNAcomics using liver samples from C57BL/6 male mice that were collected every 4 hours over a 24-hour period (12h:12h LD). Biotinylated O-GlcNAc nuclear proteins were enriched by affinity purification and then quantified using mass-spectrometry (Fig S2). To filter out non-specific proteins, unlabeled samples were processed as described above and affinity purified (Fig S2). During MS analysis, we noticed a batch effect in our 4 biological replicates of samples (Fig S3), which is a known drawback in large scale proteomics analysis [61]. Unfortunately, we were not able to run all the samples in one batch given the number of timepoints and comparisons we have in our experiments. Nonetheless, to identify as many O-GlcNAcylated proteins as possible, we

split our 4 biological replicates into two batches for bioinformatic analysis (two biological replicates in each batch) (Fig S3). To identify *bona fide* O-GlcNAcylated proteins, labeled and unlabeled samples were compared by Significance Analysis of INTeractome (SAINT) [62]. Our analysis was aimed at identifying O-GlcNAcylated proteins and quantifying global O-GlcNAcylation level over the day-night cycle, rather than identifying and quantifying O-GlcNAcylation at specific residues. The current technology to identify and quantify O-GlcNAc sites on proteins is not yet mature based on consultation with experts in the field, as the labile glycosidic bond of O-GlcNAcylation posed great challenge for mass spectrometry analysis [63]. To identify proteins with rhythmic O-GlcNAcylation with normalization to their protein expression, we performed TMT proteomic analysis to obtain the expression level of each protein (see next section) (S2, S3 Files and Fig S2). After combining the two independent batches of analysis, we identified 719 O-GlcNAcylated proteins in total, with 83 proteins (11.54%) being rhythmic (RAIN $p<0.05$) (Fig 2A and S2 File). When the threshold was set as RAIN $p<0.1$, proteins that were identified to be rhythmic increased to 136 proteins (18.92%) (Fig 2A and S2 File). Most of the protein O-GlcNAcylation were found to occur during the dark phase when mice are active (Fig 2B and C). This is consistent with the overall O-GlcNAcylation profile measured by streptavidin-HRP on Western blot (Fig 1A and B).

To identify the molecular pathways or processes that are rhythmically O-GlcNAcylated, we performed functional enrichment analysis on the proteins that we found to be rhythmically modified. We found that proteins related to gene expression were enriched (Fig S4). To further dissect out the function of the rhythmically O-GlcNAcylated proteins, we classified these proteins into protein complexes using the CORUM database [64] (S4 File). We presented the protein complexes that regulate gene expression, such as transcriptional regulation, histone modification, chromatin remodeling, and RNA processing, and plotted their daily O-GlcNAcylation levels (Fig 2D). We also included several histone acetylases and methyltransferases that do not belong to complex in CORUM but were found to exhibit rhythmic O-GlcNAcylation. Consistent with previous studies [32], CLOCK is rhythmically O-GlcNAcylated with the peak time at the end of the feeding time window (Fig 2D). It is important to note that in addition to gene-specific transcription factor complexes (Bmal1-CLOCK-CRY1/2 and E2f5-Hdac1-Rbl2 complex), more general machineries that regulate gene expression are also rhythmically O-GlcNAcylated. These include general transcriptional factors (mediator, TFIID and Brd4-TEFb complex), histone

acetylation (KAT6A), histone methylation (KDM6A, KMT2C, and NSD3), chromatin remodeling (Zipzap/p200-Srf-p49/STRAP-Nkx2.5 complex) and mRNA methylation (Cbll1-Virma-Wtap-Zc3h13 complex) (Fig 2D). Therefore, it is possible that O-GlcNAcylation could mediate the metabolic regulation of daily hepatic transcriptome by mechanisms other than directly modulating the molecular clock.

Tandem mass tag (TMT)-Mass Spectrometry (MS) profiles daily rhythm of nuclear phosphoproteome

Since both O-GlcNAcylation and phosphorylation modify serine/threonine residues on substrate proteins, many studies have been devoted to investigate G-P crosstalk [23,27,47,53,54,65,66]. Within a 24-hour period, phosphoproteome has been shown to oscillate in diverse tissue types, especially in mouse liver [55–57]. Therefore, we hypothesize that O-GlcNAcylation contributes to rhythmic liver physiology via daily G-P crosstalk. To test this hypothesis, we performed TMT phosphoproteomics to analyze daily nuclear phosphoproteome using the same tissues we used for O-GlcNAcomics analysis described above (Fig S2). We identified 19593 phosphopeptides, belonging to 3272 phosphoproteins (Fig 3A). To identify proteins with rhythmic phosphorylation independent of their protein expression, we performed a separate TMT proteomic analysis for normalization. (S3 and S5 Files). RAIN analysis showed that 2376 phosphopeptides (12.12%), corresponding to 993 phosphoproteins (30.35%), exhibit daily oscillation (RAIN $p<0.05$) (Fig 3A). Compared with previous dataset generated from label-free phosphoproteomics [55,57,58], TMT phosphoproteomics were capable of identifying more phosphopeptides (S1 Table). Interestingly, we observed that most of the phosphorylation events happen during the dark phase, coinciding with the timing of O-GlcNAcylation (Fig 3B and C). To find out the kinases that can potentially rhythmically phosphorylate the hepatic nuclear proteome, PTMphinder [67] was used to enrich phospho-motifs of phosphopeptides peaking in each phase (Fig 3C), and kinases were predicted using group-based phosphorylation site predicting and scoring (GPS) 5.0 [68]. To increase the confidence of our kinase prediction, we also selected out the kinases that are either rhythmically expressed, rhythmically O-GlcNAcylated, or rhythmically phosphorylated from our datasets (S6 File). We then classified these kinases by their phases calculated by RAIN. The circadian kinases were identified by selecting the common ones in the phase-matched rhythmic kinases in our proteomic datasets and the GPS 5.0-predicted kinase list.

We were able to find several circadian kinases that were identified in previous circadian phosphoproteomic studies [56,57], such as AKT, GSK, and CDK (Fig 3C). We also identified several circadian kinases that although have not been found in previous circadian phosphoproteomics analysis, were shown to regulate circadian rhythm via targeted analysis; they include MAPK [69], CAMK [70] and S6K [71] (Fig 3C).

Functional enrichment analysis showed that rhythmic phosphoproteome are enriched in proteins involved in transcriptional regulation, RNA processing, and chromatin organization (Fig S5). We then performed protein complex analysis to further identify the molecular pathways that are rhythmically phosphorylated (S7 File). Fig 3D illustrates protein complexes that are involved in transcriptional regulation and were found to contain multiple subunits that are rhythmically phosphorylated in our dataset. Consistent with previous findings [72], we identified core clock protein complexes, including P300-CLOCK-Bmal1 and PER2-SFPQ-SIN3A complexes (Fig 3D). Additionally, we identified several general transcriptional complexes (mediator and TFIID complexes), chromatin remodeling complexes (Ikaros and SWI/SNF complexes), and RNA processing complexes (DCS and Drosha complexes) as rhythmically phosphorylated (Fig 3D). Among phosphorylation sites we identified in this analysis, some of them have previously been characterized with functions in gene expression regulation and beyond (S2 Table). For other sites with unknown functions, we identified the phosphorylation events locating in or adjacent to functional domains based on PhosphoSitePlus database and these novel sites could have potential functions regulating liver physiology (S3 Table). Taken together, our data suggest that the daily rhythm of the phosphoproteome could regulate the rhythmic hepatic transcriptome.

Crosstalk between O-GlcNAcylation and phosphorylation (G-P) regulates hepatic protein function

O-GlcNAcylation can occur at the same residues or adjacent residues targeted by phosphorylation to regulate phosphorylation events [23,27,47,53,54,65,66]. Since both O-GlcNAcylation and phosphorylation were found to oscillate over a day-night cycle, we sought to identify rhythmic phosphorylation events that can be potentially regulated by daily O-GlcNAcylation rhythm of substrate proteins. By comparing the rhythmic O-GlcNAcome and phosphoproteome, we found 14 proteins exhibiting both rhythmic O-GlcNAcylation and phosphorylation (Fig 4A). Spearman correlation analysis between overall O-GlcNAcylation of the

proteins and each phosphorylation peptides of the same proteins showed that most of the O-GlcNAcylation and phosphorylation on proteins are positively correlated (Fig 4A), indicating the two PTMs potentially facilitate each other. However, a smaller portion of the O-GlcNAcylation and phosphorylation on proteins are negatively correlated, suggesting these two PTMs can also inhibit each other in these cases (Fig 4A). Similarly, phase analysis showed that most of the O-GlcNAcylation and phosphorylation occur simultaneously over the 24-hour day-night cycle (Fig 4B). Analysis on individual phosphopeptide showed that some phosphorylation happens in phase with O-GlcNAcylation (i.e. positive correlations), such as pCLOCK(T461) (Fig 4C) and pARID1A(S1607/S1609) (Fig 4D), while other phosphorylation events are out of phase with O-GlcNAcylation (i.e. negative correlations), as exemplified by pRBL2(S935/S937) (Fig 4F) and pZC3H13(S949) (Fig 4G). pRSRC1(S6), and pRSRC1(S50/S52) demonstrate the situation that depending on the specific sites on even a single substrate protein, O-GlcNAcylation and phosphorylation can be in phase (Fig 4F) or out of phase (Fig 4I). Additionally, protein complex analysis identified 4 protein complexes out of these 14 proteins with both rhythmic O-GlcNAcylation and phosphorylation, including transcription factor complexes (Arntl-Clock-Cry1/2 complex, TFIID complex and E2f5-Hdac1-Rbl2 complex) and an RNA processing complex (Cbll1-Virma-Wtap-Zc3h13 complex). Our data suggest that G-P crosstalk contributes to regulation of rhythmic protein function in mouse liver.

Daily G-P crosstalk on CLOCK and RBL2

To gain a deeper understanding of the potential crosstalk between O-GlcNAcylation and phosphorylation over a 24-hr period, we asked whether proteins with rhythmic phosphorylation and O-GlcNAcylation identified in our studies harbor G-P interplay motifs [65,66]. We found eight phosphorylation sites that harbor three different G-P interplay motifs (Fig 5A), where O-GlcNAcylation and phosphorylation either compete for the same modification site or have inhibitory effects when in close proximity. Among these eight phosphorylation sites, the functions of two, namely CLOCK(S431) [73] and RBL2(S659) [74,75], have been characterized.

CLOCK(S431) is the priming phosphorylation site for glycogen synthase kinase-3 (GSK3). Once CLOCK(S431) is phosphorylated, GSK3 phosphorylates S427, which promotes the degradation of CLOCK [73]. Given global O-GlcNAcylation of CLOCK has been shown to increase its stability [32], we hypothesize that O-GlcNAcylation stabilizes CLOCK in a time-of-

day manner by competing with S431 phosphorylation to inhibit S427 phosphorylation (Fig 5B). To validate the daily CLOCK O-GlcNAcylation rhythm detected in our mass spectrometry-based O-GlcNAcomics analysis, we applied a targeted chemoenzymatic labeling approach to profile daily CLOCK O-GlcNAcylation level. Consistent with the results from untargeted O-GlcNAcomic analysis, CLOCK O-GlcNAcylation exhibits robust daily rhythmicity (Fig 5C and D, S6A). Although we detected S431 phosphorylation on multiple peptides in our dataset, the S431 phosphorylation always co-occurs with nearby phosphorylation events, making it difficult to quantify the actual level of S431 phosphorylation. We instead used S427 phosphorylation as the functional readout for the competition between O-GlcNAcylation and phosphorylation at S431. When we overlaid CLOCK O-GlcNAcylation rhythm from targeted analysis with the daily phosphorylation level at S427, we observed out of phase relationship (O-GlcNAcylation: ZT20; pS427: ZT8, RAIN). Between ZT7 and ZT11, when CLOCK O-GlcNAcylation level is low, S427 phosphorylation level remains high. The opposite is observed during the night period (ZT19) (Fig 5D). These observations support that CLOCK O-GlcNAcylation and S427 phosphorylation do not co-occur and CLOCK O-GlcNAcylation inhibits S427 phosphorylation.

As CLOCK S427 phosphorylation promotes degradation of CLOCK, we assayed CLOCK protein level over a 24-hr cycle using Western blots (Fig 5C). The daily CLOCK protein levels detected in our proteomic dataset and Western blots has similar trends with minor difference at ZT4 (Fig S6B). We then compared levels of daily S427 phosphorylation and CLOCK protein (Fig 5E). As S427 phospho-occupancy rises and maintains a relatively high level between ZT3 and ZT11, CLOCK protein level decreases (Fig 5E). Between ZT15 and ZT23, CLOCK phosphorylation level rises again, while CLOCK protein level stays low. All these observations support the conclusion that daily rhythms of S427 phosphorylation contributes to the oscillation of CLOCK protein abundance. Since S427 is known to be phosphorylated by GSK3, we investigated the phosphorylation status of GSK3 as an indicator of its kinase activity utilizing our TMT phosphoproteomic dataset. We found daily rhythms in the phospho-occupancy of GSK3α(S21), whose phosphorylation inhibits the kinase activity of GSK3α [76] (Fig 5F). Consistent with our hypothesis, daily rhythmicity of pGSK3α(S21) and pCLOCK(S427) are out of phase (pGSK3α(S21): ZT24; pCLOCK(S427): ZT8, RAIN). In summary, our results suggest that daily CLOCK O-GlcNAcylation rhythm together with GSK3α(S21) phosphorylation rhythm could synergistically regulate CLOCK stability by influencing daily phospho-occupancy at S427.

Mouse RBL2(S659) is homologous to RBL2(S662) in human. Upon sequence alignment, we found that this phosphorylation site belongs to a phospho-cluster (mouse RBL2 aa636-669) with 94.11% conservation between mouse and human. The phosphorylation of mRBL2(S659) together with S669 and S636 can potently disrupt the interaction between RBL2 and E2F4, which derepress the expression of RBL2-E2F4 target genes and facilitate the progression of cell cycle [74,75]. Interestingly, a short peptide of hRBL2 (aa655-667), containing mouse T662 homologous residue, was shown to be O-GlcNAcylated, although the exact O-GlcNAc site is unknown [77]. Our G-P interplay motif analysis suggests that T662 is a potential O-GlcNAc site, whose occupancy inhibits phosphorylation at S659 (Fig 5G). We therefore hypothesize that rhythmic O-GlcNAcylation of RBL2 can drive rhythmic phosphorylation at S569 to regulate RBL2-E2F4 target gene expression. To test our hypothesis, we analyzed daily rhythms of RBL2 O-GlcNAcylation and S659 phosphorylation. We observed a slightly earlier phase of RBL2 O-GlcNAcylation rhythm as compared to that of S659 phosphorylation (Fig 5H). O-GlcNAcylation level is significantly higher than pS659 at ZT11 ($p<0.05$, two-way ANOVA with post-hoc test), indicating that RBL2 O-GlcNAcylation could potentially inhibit S659 phosphorylation. To investigate whether rhythmic phosphorylation at S659 contributes to the rhythmic expression of RBL2-E2F4 target genes, we plotted the mRNA pattern of a target gene of RBL2-E2F4 complex from Greco et al. [78], *E2f2* [79,80]. Notably, the age and gender of mice, TRF treatment, and collection time points in Greco et al. [78] are very similar to that in our experiments, allowing us to assess the relationship of RBL2 PTM and target gene expression pattern. As described above, the phosphorylation of RBL2 S659 is expected to promote the expression of RBL2-E2F4 target genes. In support of this hypothesis, we observed a very similar trend between S659 phosphorylation and *E2f2* mRNA rhythms (Fig 5I). In summary, our data suggest rhythmic O-GlcNAcylation of RBL2 could drive daily phosphorylation of RBL2(S659), which could lead to rhythmic dissociation of RBL2 and E2F4 and rhythmic expression of RBL2-E2F4 target genes, such as *E2f2*.

In addition to the 14 proteins with both oscillating O-GlcNAcylation and phosphorylation, we expect that O-GlcNAc sites on more proteins could interact with rhythmic phosphosites, given that the overall O-GlcNAcylation status of proteins detected in our global O-GlcNAcylation analysis may underestimate potential rhythmicity of individual O-GlcNAc sites. Future detection of individual O-GlcNAcylation events could reveal additional G-P crosstalk. Nevertheless, to

encourage future studies on more daily G-P crosstalk, we took a subset of rhythmic phosphorylated proteins that are also O-GlcNAcylated in our O-GlcNAcomic dataset, and searched whether these rhythmic phosphosites belong to any G-P interplay motifs. We found 86 phosphosites within G-P motifs on 53 proteins (S8 File). These 53 proteins include components in general transcription machinery (MED13/14, PCF11, and CDK13), gene-specific transcription factors (NFIL3, HNF1a, CEBPB, TRIM24, etc.), histone modification (SETD1A, EP400, and GATAD2A/B), chromatin remodeling (SMARCC2, HIRA, and BRD8), RNA processing (ZC3H13, and FIP1), and nucleo-cytoplasmic transportation (POM121 and NUP214) (S8 File). We therefore conclude that G-P crosstalk is expected to play a significant role in regulating time-specific function of proteins and shape daily rhythm in hepatic transcriptome.

O-GlcNAcylation of nuclear proteins in liver regulates daily hepatic transcriptome

Given rhythmic O-GlcNAcylated proteins are enriched with proteins involved in the regulation of gene expression, we compared our rhythmic O-GlcNAcome to their rhythmically expressed target genes from Greco et al. [78] to obtain functional insights into the role of rhythmic O-GlcNAcome. To identify the target genes of each O-GlcNAcylated transcription factor, we referred to the TFLink database [81], the most recent and comprehensive database for transcription factor-target gene interactions. We performed spearman correlation analysis between the O-GlcNAcylation rhythm of transcription factors and their target gene expression and observed that O-GlcNAcylation of transcription factors could be positively or negatively correlated to the expression level of target genes, depending on each target genes (Fig 6A). This indicates that not surprisingly the function of O-GlcNAcylation on transcription factors is target-specific. Notably, the expression of the target genes is also regulated by other transcriptional complexes, local chromatin state, and DNA methylation, etc. Future functional analysis will be necessary to investigate the function of individual O-GlcNAcylation events on substrate transcription factor function.

It is likely that hepatic gene expression could be indirectly regulated by O-GlcNAcylation through G-P crosstalk on transcription factors. We performed spearman correlation analysis between the target gene expression and rhythmic O-GlcNAcylation and G-P interactive phosphorylation of transcription factors. By comparing the correlation patterns between the two PTMs on each protein, we observed that CLOCK O-GlcNAcylation could have similar function

as all the phosphorylation events except for pCLOCK(S406), while O-GlcNAcylation of RRD2 and SALL1 could have opposite function compared to the phosphorylation events on the same proteins (Fig 6B). However, there is mixed results for the functional estimation of TAF10 O-GlcNAcylation and pTAF10(S44). Therefore, we conclude that target gene expression of a given transcription factor could be differentially regulated by its O-GlcNAcylation and phosphorylation. In these cases, site-specific characterization of specific O-GlcNAcylation and phosphorylation is necessary to interpret the functional outcome of the two PTMs.

Food intake at unnatural day feeding time in mice disrupts protein O-GlcNAcylation rhythm

We previously showed that O-GlcNAcylation is regulated by both feeding-fasting cycles and the molecular clock in flies [30]. We hypothesize that timing of food intake could affect daily O-GlcNAcylation rhythm in mouse liver. To test this hypothesis, we subjected mice to unnatural day time-restricted feeding (DRF) and compared their nuclear protein O-GlcNAcylation pattern with NRF mice (Fig 7A). Mice treated with DRF lost their daily O-GlcNAcylation rhythm, and the global O-GlcNAcylation level of hepatic nuclear proteins remained at a relatively high level through the day-night cycle (Fig 7B and C).

To investigate whether the altered O-GlcNAcylation rhythm in DRF mice results from altered daily UDP-GlcNAc rhythm, we used targeted metabolomics to detect UDP-GlcNAc levels in livers of mice fed under NRF and DRF. Our results showed that DRF mouse liver exhibited dampened daily UDP-GlcNAc rhythmicity and the level of UDP-GlcNAc remained at a higher level overall when compared to that in NRF mouse liver, suggesting altered UDP-GlcNAc level likely contributed to altered O-GlcNAcylation in DRF mice liver (Fig 7D). To rule out the possibility that the altered UDP-GlcNAc levels in DRF mouse liver is due to increased food intake, we measured daily total food consumption of NRF and DRF mice. We did not observe a significant increase in food consumption in the DRF group. DRF group instead fed slightly less than NRF group, indicating that food consumption is not the major cause of increased UDP-GlcNAc level (Fig 7E). In conclusion, timing of food intake affects O-GlcNAcylation rhythm in mouse liver partially by influencing the level of UDP-GlcNAc.

Discussion

In this study, we investigated the contribution of nutrient-sensitive O-GlcNAcylation as a post-translational mechanism to regulate rhythmic hepatic gene expression. Despite a substantial body of work showing that the rhythmic hepatic transcriptome is highly responsive to the timing of food intake [11,14,15,19–22], our understanding of the mechanisms by which rhythmic feeding-fasting activity regulates genome-wide gene expression is far from complete. Here, we showed that nuclear proteins in mouse liver exhibit rhythmic O-GlcNAcylation over a 24-hour day-night cycle when mice were fed at natural night feeding time (Fig 1). Global O-GlcNAcomics analysis showed that proteins involved in transcriptional regulation, histone modification, chromatin remodeling and RNA processing are enriched among rhythmically O-GlcNAcylated proteins (Fig 2). Combining results from targeted metabolomics, phosphoproteomics, biochemistry and G-P interplay motif analysis, we formulated a model showing the role of O-GlcNAcylation in mediating the effect of metabolic input on the daily hepatic transcriptomic rhythm (Fig 8). We propose that environmental cues signaling via the molecular clock and the timing of metabolic input from food intake converge to regulate daily rhythm in the O-GlcNAcome. O-GlcNAcylation targeting the same site or adjacent site have the potential to affect phosphorylation, as exemplified by CLOCK and RBL2 respectively. Therefore, O-GlcNAcylation can shape daily transcriptomic rhythm by either directly modulating proteins involved in regulation of gene expression or in an indirect manner by interacting with phosphorylation of these proteins.

To infer the function of the rhythmic O-GlcNAcome, we established correlations between O-GlcNAcylation rhythms on transcription factors with mRNA expression rhythms of their target genes. Not surprisingly, we found that these correlations to be highly mRNA-specific. We expect that this is because many other mechanisms, such as chromatin status, DNA methylation, coordination with transcriptional protein complexes, and mRNA processing [82–84] also regulate the levels of steady state mRNA. Nonetheless, previous studies showed that O-GlcNAcylation modulates functional outcomes of several transcription factors detected in our rhythmic O-GlcNAcome [44,85,86]. O-GlcNAcylation of FOXO3 at S284 suppresses the expression of *p21*, one of its target gene [86]. Ten-eleven translocation 3 (TET3) involved in nuclear DNA demethylation has been shown to be O-GlcNAcylated and promotes nuclear export of TET3 [44]. Therefore, it is possible that the time-of-day specific functions of these proteins driven by rhythmic O-GlcNAcylation contribute to daily transcriptomic rhythm. To more fully understand the function of O-GlcNAcylation on rhythmic gene expression, identification of O-GlcNAcylation sites and

future mechanistic studies are warranted to characterize the function of oscillating O-GlcNAcylation on individual transcription factors, chromatin modifiers, and RNA splicing factors.

Since there exists crosstalk between O-GlcNAcylation and phosphorylation at the same or adjacent site on its protein substrate, we investigated the possibility that rhythmic O-GlcNAcylation can interact with phosphoproteome to regulate the hepatic transcriptome. Given that many of the 14 proteins harboring G-P interplay motifs are known to play important roles in various cellular processes, such as transcriptional regulation (TAF10, SALL1, and ZNF148), RNA processing (ZC3H13, CPSF7, RSRC1, and ZFC3H1), chromatin modification (ARID1A, NFRKB, and BRD2), and cell cycle regulation (LIN54), it is certainly important to understand how daily G-P crosstalk could modulate the activities of these proteins to regulate daily hepatic physiology. Additionally, a broader motif search on O-GlcNAcylated proteins with rhythmic phosphorylation showed that 86 rhythmic phosphosites could potentially be regulated by G-P interplay motifs (S8 File). Although proteomic analysis to identify O-GlcNAcylation sites is still quite challenging at present [63], future attempts will be necessary to reveal the interplay of O-GlcNAc sites and phosphosites that cannot be identified through G-P motif predictions.

Our results showed that O-GlcNAcylation is rhythmic in mouse liver with a peak phase that aligns with timing of food intake. Given the nutrient-sensitive property of O-GlcNAcylation, it is perhaps not surprising to observe similar phenomenon in mouse heart [29] and fly body [30]. Therefore, O-GlcNAcylation may represent a conserved mechanism by which nutrient input regulates daily protein functions under natural feeding conditions. We observed that unnatural feeding time (DRF) dampens the global O-GlcNAcylation rhythm of hepatic nuclear proteins, instead of shifting the phase of O-GlcNAcylation to align with the altered feeding period. Given that O-GlcNAcylation is also responsive to the molecular clock [30], it is likely that clock-controlled mechanisms prevent lowering of O-GlcNAcylation level at specific time of day (Fig 8). Furthermore, the transcriptomic response to unnatural feeding time in mouse have been shown to be organ-specific. Adipose tissue and liver are highly responsive to timing of food intake, while kidney and heart are less responsive [11]. Therefore, it is possible that the unnatural feeding activity could have tissue-specific effects on daily O-GlcNAcylation rhythm, which then contributes to the tissue-specific differential regulation of transcriptome by timing of food intake. To test this hypothesis, future studies are necessary to investigate how O-GlcNAcylation rhythms are regulated by metabolic signals from feeding activity across tissues.

We studied daily nuclear O-GlcNAcome as a mechanism to mediate the nutrient sensitivity of daily hepatic transcriptomic rhythm. O-GlcNAcylation of cytoplasmic proteins are also likely to oscillate. O-GlcNAcylation of cytoplasmic proteins can regulate biological processes such as translation and immune response [23,26], and relay signals into nucleus via signaling pathways [20,21,87,88]. Despite our understanding on O-GlcNAcylation regulation of nutrient-sensitive signaling pathways, such as those involving mTOR [89], AMPK [90,91], and insulin [92], whether O-GlcNAcylation coordinates with these nutrient-sensitive signaling pathways and other nutrient-sensitive PTMs in a time-of-day manner remains to be investigated. Furthermore, we observed that unnatural feeding time can alter daily rhythms of bile acids and S-adenosylmethionine (SAM) (Fig S7). Bile acid can regulate gene expression through a nuclear receptor, farnesoid X receptor (FXR) [16,93], and SAM is the substrate for methylation of DNA, RNA and proteins [94]. Therefore, a comprehensive understanding of metabolic regulation of daily physiological rhythms will require investigations into more nutrient-sensitive mechanisms.

In summary, we showed that O-GlcNAcylation exhibits daily oscillation in hepatic nuclear proteins in mice and feeding mice at unnatural feeding time disrupts daily O-GlcNAcylation rhythm. Using proteomic approaches, we identified nuclear proteins exhibiting rhythmic O-GlcNAcylation and evaluated G-P crosstalk at the proteomic level over a day-night cycle. Finally, our findings on CLOCK, a protein in the core molecular clock loop, and RBL2, a key transcription factor in regulating cell cycle, were used to highlight the daily crosstalk between O-GlcNAcylation and phosphorylation and its rhythmic functional outcomes. Our results provide new insights into metabolic regulation of daily biological rhythms at the PTM level and shed light on the deleterious effects of improper mealtimes.

Materials and Methods

Animal treatments and collection of liver samples

All experiments including animal feeding, treatment, and tissue collection were carried out in accordance with the guidelines of Institutional Animal Care and Use Committees (IACUC) of the University of California, Davis. C57BL/6 male mice were ordered from JAX laboratory at the age of 6 weeks. Mice were first entrained for 2 weeks *ad libitum* in 12h light:12h dark cycle. Mice were then randomized into two time-restricted feeding (TRF) groups: night restricted feeding (NRF) between ZT12-24 (ZT, zeitgeber time; ZT0 indicates light on, while ZT12 indicates light

off) and day restricted feeding (DRF) between ZT0-12. Normal chow food was provided in the above time-restricted feeding treatments and food intake was measured by comparing the food weight before and after each feeding window. The mice were TRF-treated for three weeks. Three weeks is enough time for DRF group to adapt to the new feeding window and fed comparable amount as NRF group [95]. It also allows the entrainment of the hepatic clock to be complete [14,15] and the rhythmic transcriptome would be altered [11]. After TRF treatment, mice were sacrificed every 4 hours over a 24-hour period and liver samples were collected. Samples were then flash frozen in liquid nitrogen, ground into powders and stored at -80 °C until sample processing.

Extraction of mouse liver nuclei proteins

Mouse liver nuclei were extracted according to Nagata et al. [96] with the following modifications. Liver samples were dounced in Buffer A (250mM sucrose, 10mM Tris HCl pH7.5, 5mM $MgCl_2$,100µM PUGNAc, and Roche EDTA-free protease inhibitor cocktail) with a loose pestle. The suspension was passed through a cell strainer (70µm pore size, Fisher Scientific, Hampton, NH) by centrifuging at 300g for 1 min at 4°C. The crude nuclei were pelleted by centrifugation at 600g for 15 mins at 4°C. To further purify the crude nuclei, the pellets were resuspended in 9 volumes of ice-cold Buffer B (2M sucrose, 1mM $MgCl_2$, and 10mM Tris HCl pH7.5) and were then centrifuged at 16000g for 15 mins. The supernatant was discarded and the pure nuclear pellets were resuspended in boiling buffer (100mM Tris pH8.0, 2% SDS, 100µM PUGNAc, and Roche EDTA-free protease inhibitor cocktail) [59]. Nuclear proteins were extracted by heating at 95°C for 5 min. After centrifuging at 16000g for 5 mins to separate the soluble and non-soluble nuclear fractions, the nuclear protein lysate was transferred to a new tube.

Expression and purification of bovine β-1,4-galactosyltransferase 1 (GalT1 Y289L)

GalT1 (Y289L), the chemoenzymatic labeling enzyme for detecting O-GlcNAcylated proteins, was expressed and purified according to Thompson et al. [59] The bovine GalT1 was obtained from Genomics-online (Cat#: ABIN3462403) and GalT1 tyrosine 289 is mutated into leucine to increase its activity for the chemoenzymatic labeling reaction [97,98]. GalT1(Y289L) was subcloned into pET22-6xHis vector and transformed into BL21(DE3) competent cells for expression of the GalT1(Y289L) protein. The harvested cells were lysed in PBS containing 1mM

EDTA by sonication. After centrifuging at 14000g for 30 min, the pellet was collected given GalT1(Y289L) is insoluble in PBS. The pellet was suspended in wash buffer (1xPBS, 25% sucrose, 1mM EDTA, and 0.1% Triton X-100) and spun down; this was repeated 5 times. The pellet was then resuspended in PBS containing 1mM EDTA and this was repeated twice to remove detergent. After the last centrifuge step, the pellet was resuspended in denaturing buffer (5M guanidine hydrochloride, 0.3M sodium sulfite) and treated with S-sulfonating agent, 2-Nitro-5-thiosulfobenzoate (NTSB). Ice-cold water was added to precipitate the GalT1(Y289L) protein and the mixture was centrifuged at 10,000g for 10 min. This step was repeated 3 times to remove residual NTSB. The final pellet was resuspended in 5M guanidine hydrochloride and diluted 10 times in refolding buffer (0.5M L-arginine, 50mM Tris pH8.0, 5mM EDTA, 4mM cysteamine, and 2mM cystaminea). The resulting GalT1(Y289L) solution was dialyzed in dialysis buffer (50mM Tris pH8.0, 5mM EDTA, 4mM cysteamine, and 2mM cystamine) and concentrated to 2mg/ml.

Chemoenzymatic labeling of O-GlcNAcylated proteins

Chemoenzymatic labeling of O-GlcNAcylated nuclear proteins was performed according to Thompson et al. [59] with the following modifications. The nuclear protein lysate was quantified and 100µg protein was used for labeling. Protein lysate was treated with 25mM DTT at 95°C for 5 mins and 50mM iodoacetamide at room temperature for 1 hour in the dark. Proteins were precipitated using chloroform-methanol method and dissolved in 40µl 1% SDS with 20mM HEPES pH7.9 by heating up at 95°C for 5 mins. The O-GlcNAc group was first labeled with azide in the labeling buffer (20mM HEPES pH7.9, 50mM NaCl, 2% IGEPAL-CA630, 25µM PUGNAc, 25mM NaF, 0.5mM PMSF, 5.5 mM $MnCl_2$, 25µM UDP-GalNAz, 50µg/ml GalT1(Y289L), and Roche EDTA-free protease inhibitor cocktail). To remove the labeling reagents, proteins were precipitated using chloroform-methanol method and dissolved in 37.5µl 1% SDS with 20mM HEPES pH7.9. Biotin was attached to the azide group in the biotinylation buffer (1xPBS, 100µM biotin alkyne, 2mM sodium ascorbate, 100µM Tris (benzyltriazolylmethyl) amine, and 1mM $CuSO_4$). To prepare for Western blot after O-GlcNAc labeling, samples were precipitated and dissolved in 50µl 1% SDS with 20mM HEPES pH7.9. O-GlcNAc proteins were detected using α-streptavidin-HRP (Cell Signaling Technologies, Danvers, MA) (1:10000). For background

deduction, unlabeled samples were processed in parallel with GalT1(Y289L) excluded in the labeling buffer.

Targeted gas chromatography coupled to time-of-flight (GC-TOF) mass spectrometry (MS) analysis and HILIC-TripleTOF MS/MS analysis

10mg liver samples were analyzed using GC-TOF MS and HILIC-TripleTOF MS/MS approaches as previously described [30,99]. Samples were extracted with acetonitrile/isopropanol/water 3:3:2 (v/v/v). For GC-TOF MS analysis, 0.5µl samples were injected into an Agilent 6890 gas chromatograph (Agilent, Santa Clara, CA) and analyzed using a Leco Pegasus IV time of flight mass (TOF) spectrometer. Result files were processed using the metabolomics BinBase database. For HILIC-TripleTOF MS/MS, 5µl samples were injected onto a Waters Acquity UPLC BEH Amide column (Waters, Milford, MA) and analyzed using a 1x 6600 TripleTOF high resolution mass spectrometer (SCIEX, Framingham, MA). Mass spectra were analyzed and interpreted using MS-DIAL v3.90 [100]. Peak heights from both analyses were reported as quantification. Standard compounds from the hexosamine biosynthesis pathway (HBP) were diluted into multiple concentrations and analyzed in parallel to generate standard curves. The concentration of each detectable HBP metabolites in liver samples was then calculated based on the peak height and standard curves.

Sample preparation for O-GlcNAcomics

Nuclear proteins were chemoenzymatically labeled as described above with 1mg protein per samples. After the final precipitation, samples were dissolved in 400µl 1% SDS with 50mM Tris pH7.5. 600µl supplementary buffer (50mM Tris pH7.5, 375mM NaCl, and 2.5% IGEPAL-CA630) was added to dilute protein into immunoprecipitation (IP) buffer (50mM Tris pH7.5, 150mM NaCl, 0.4% SDS, and 1% IGEPAL-CA630). The protein sample is quantified using Qubit before IP. O-GlcNAc proteins were immunoprecipitated using Dynabeads™ MyOne™ Streptavidin T1 (Fisher Scientific) and the IP reactions were incubated at room temperature for 2 hours. The beads were washed with wash buffer (50 mM Tris pH7.5, 400 mM NaCl, 1% IGEPAL-CA630, and 0.4% SDS) for 5 times and 50mM NH_4HCO_3 for 8 times. After removing all the solutions through magnetic separation, beads were stored at -80°C prior to mass spectrometry

analysis. To identify non-specific binding, unlabeled samples were processed in parallel with GalT1(Y289L) excluded in the labeling buffer.

Mass spectrometry (MS) to identify O-GlcNAc proteins

The bead-bound proteins were digested on beads according to Mohammed et al. [101]. Briefly, samples were digested using 10µl (10ng/µl) of trypsin in 100 mM NH_4HCO_3 overnight at 37 °C. Another 10µl (10ng/µl) of trypsin in 100 mM NH_4HCO_3 was added the next day to further digest for 4 hours. The digested peptides were extracted twice with 5% formic acid and 60% acetonitrile.

Samples were analyzed by liquid chromatography–mass spectrometry (LC–MS) according to Sharma et al. [102]. The Nano-LC-MSMS was performed using a Dionex rapid-separation liquid chromatography system interfaced with an Eclipse (Fisher Scientific). Samples were loaded onto a fused silica trap column (Acclaim PepMap 100, 75 µm × 2 cm, Fisher Scientific) and washed for 5 min at 5 µl/min with 0.1% TFA. An analytical column (Nanoease MZ peptide BEH C18, 130A, 1.7 µm, 75 µm× 250 mm, Waters, Milfored, MA) for LC-MS/MS was brought in-line with the trap column. A segmented linear gradient was used to fractionate peptides at 300nl/min: 4–15% solution B in 30 min (solution A: 0.2% formic acid, and solution B: 0.16% formic acid, 80% acetonitrile), 15–25% solution B in 40 min, 25–50% solution B in 44 min, and 50-90% solution B in 11 min. Before the next run started, solution B should return to 4% for 5 min. Data-dependent acquisition procedure was applied to acquire the spectrometry data. A cyclic series of a full scan were performed with a resolution of 120,000. The 20 most intense ions were analyzed by MS/MS (higher-energy collisional dissociation (HCD), relative collision energy 27%) with a dynamic exclusion duration of 20s.

LC-MS/MS data were analyzed with Thermo Proteome Discoverer 2.4 (Fisher Scientific) into MASCOT Generic Format (MGF). The resulting peak list was searched against Uniprot mouse database and a database consisted of common lab contaminants (CRAP) using in house version of X!Tandem (GPM Fury [103]). During searching, fragment mass error was set at 20 ppm and parent mass error was set at ±7 ppm. Carbamidomethylation on cysteine was set as fixed modification. In primary search, methionine monooxidation was set as variable modifications, while in refinement search, asparagine deamination, tryptophan oxidation and dioxidation, methionine dioxidation, and glutamine to pyro-glutamine were included. Protease was set as

trypsin C-terminal of R/K unless followed by P with 1 miscut allowed during the preliminary search and 5 miscuts allowed during refinement. For minimum acceptable peptide and protein expectation scores, 10−2 and 10−4 were respectively applied. The overall peptide false-positive rate was set to 0.07% [104].

Tandem mass tag (TMT)-MS for phosphoproteomics

For parallel phosphoproteomic analysis using the same mouse livers used for O-GlcNAcomics analysis, mouse liver nuclei were extracted as described above. The nuclear pellets were resuspended in 2x laemmili buffer with 50 mM DTT. Nuclei were sonicated, followed by incubating at 95 °C for 10 min. After centrifugation at 25000g for10 min at 4 °C, the soluble fraction was saved in a new tube, while the insoluble fraction was further extracted using 8 M Urea. The insoluble fraction was centrifuged again, and the supernatant was combined with the soluble fraction. Protein concentration was determined by Pierce™ 660nm Protein Assay Kit (Fisher Scientific). 300µg of lysate were run into SDS-PAGE for TMT-MS analysis. We chose to use TMT labeling method to increase the comparability of samples [105]. However, as the currently available TMT labeling method can maximumly label 18 samples (TMTpro-18plex) in one run, we were only able to process 3 biological replicates of mouse livers [105].

The gel slices were incubated with 10 mM DTT at 60°C for 30 min, and then with 20 mM iodoacetamide at room temperature for 1 hour in dark. The samples were digested by trypsin at 1:50 (w:w, trypsin:sample) and incubated at 37°C overnight. The digested peptides were extracted and dried under vacuum and washed with 50% acetonitrile to pH neutral. The digested peptides were labeled with Thermo TMT18plex (Lot# for TMTpro16: XA341491; Lot# for last two channels: XA338617) followed by the manufacture's protocol. Labeled samples were pooled at 1:1 ratio for a small volume and analyzed with LC-MS/MS to get normalization factor. The labeling efficiency is 97.9%. Based on the normalization factor, the samples were pooled together and desalted with SepPack tC18 columns (Varian, WAT054960).

The desalted samples were fractionated by high-pH RPLC chromatography using Agilent 1100 series. The samples were solubilized in 200 µl of 20 mM ammonium (pH10), and injected onto an Xbridge column (Waters, C18 3.5 µm 2.1X150 mm) using a linear gradient of 1%B/min from 2-45% of B (buffer A: 20 mM ammonium, pH10, B: 20 mM ammonium in 90% acetonitrile, pH10). UV 214 was monitored. 1 min fractions were collected. 5% of fractions 29 to 46 was saved

for proteome analysis and the rest of all fractions were dried until there is around 50µl left for each fraction. Then the fractions were combined and dry completely under speed vacuum for phosphopeptide enrichment.

IMAC enrichment of phosphopeptides was adapted from Mertins et al. [106] with modifications. Ion-chelated IMAC beads were prepared from Ni-NTA Superflow agarose beads (Qiagen, MA). Nickel ion was stripped with 50mM EDTA and iron was chelated by passing the beads through aqueous solution of 200mM $FeCl_3$ followed by three times of water wash and one time wash with binding buffer (40% acetonitrile, 1% formic acid). The combined basic RP fractions were solubilized in binding buffer and incubated with IMAC beads for 1 hour. After three times of wash with binding buffer, phosphopeptides were eluted with 2x beads volume of 500mM potassium hydrogen phosphate, pH7.0 and the eluate was neutralized with 10% formic acid. The enriched phosphopeptides were further desalted by Empore 3M C18 (2215) StageTip[2] prior to nanoLC-MS/MS analysis.

Nano-LC-MSMS was performed using a Dionex rapid-separation liquid chromatography system interfaced with an Eclipse (Fisher Scientific). The enriched phosphopeptides and selected desalted fractions 29-46 were loaded onto an Acclaim PepMap 100 trap column (75µm x 2cm, Fisher Scientific) and washed with Buffer A (0.1% trifluoroacetic acid) for 5 min with a flow rate of 5µl/min. The trap was brought in-line with the nano analytical column (nanoEase, MZ peptide BEH C18, 130A, 1.7um, 75umx20cm, Waters) with flow rate of 300nL/min with a multistep gradient (4% to 15% buffer B [0.16% formic acid and 80% acetonitrile] in 20 min, then 15%–25% B in 40 min, followed by 25%–50% B in 30 min). The scan sequence began with an MS1 spectrum (Orbitrap analysis, resolution 120000, scan range from 350–1600 Th, automatic gain control (AGC) target 1E6, maximum injection time 100 ms). The top S (3 sec) duty cycle scheme were used for determining number of MSMS performed for each cycle.

For proteomic samples, SPS method was used. Peptide ions were first collected for MS/MS by collision-induced dissociation (CID) and analyzed in quadrupole ion trap analysis (automatic gain control (AGC) 2E4, normalized collision energy (NCE) 35, maximum injection time 120 ms, and isolation window at 0.7). Following acquisition of each MS2 spectrum, 10 MS2 fragment ions were captured in the MS3 precursor population using isolation waveforms with multiple frequency notches. MS3 precursors were fragmented by HCD and analyzed using the Orbitrap (NCE 55, AGC 1.5E5, maximum injection time 150 ms, resolution was 50,000 at 400 Th).

For phosphopeptide, MS/MS method was used. Parent masses were isolated in the quadrupole with an isolation window of 0.7m/z, AGC 1E5, and fragmented with HCD with a normalized collision energy of 34%. The fragments were scanned in Orbitrap with resolution of 50000. The MS/MS scan ranges were determined by the charge state of the parent ion but lower limit was set at 110 amu.

LC-MS/MS data were analyzed with Proteome Discoverer 2.4 (Fisher Scientific) with sequent search engine against Uniprot mouse database and a database consisted of common lab contaminants. For proteome data, The MS mass tolerance was set at ±10ppm, MS/MS mass tolerance were set at ±0.4Da. TMTpro on K and N-terminus of peptides and carbamiodomethyl on cysteine was set as static modification. Methionine oxidation, protein N-terminal acetylation, N-terminal methionine loss or N-terminal methionine loss plus acetylation were set as dynamic modifications. Protease was set as trypsin digest with 2 miscuts allowed. For phosphopeptide enriched sample runs, The MS mass tolerance was set at ±10ppm, the MS/MS mass tolerance were set at ±0.02Da. TMTpro on K and N-terminus of peptides and carbamiodomethyl on cysteine was set as static modification. Serine, threonine, and tyrosine phosphorylation, methionine oxidation, protein N-terminal acetylation, N-terminal methionine loss or N-terminal methionine loss plus acetylation were set as dynamic modifications. Protease was set as trypsin digest with 2 miscuts allowed. Percolator was used for results validation. Concatenated reverse database was used for target-Decoy strategy. High confidence for protein and peptides were defined as FDR<0.01, medium confidence was defined as FDR <0.05.

For reporter ion quantification, reporter abundance was set to use signal/noise ratio (S/N) if all spectrum files have S/N values. Otherwise, intensities were used. Quan value was corrected for isotopic impurity of reporter ions. Co-isolation threshold was set at 75%. Average reporter S/N threshold was set at 10. SPS mass matches percentage threshold was set at 65%. Protein abundance of each channel was calculated using summed S/N of all unique+razor peptide. For proteome data, the abundance was further normalized to summed abundance value for each channel over all peptides identified within a file. The same normalization factors were also used to normalize phosphopeptide abundance. Following the analytic method of TMT phosphoproteomics dataset in Li et al. [107], each phosphopeptide was further normalized to corresponding master protein abundance value if the protein group also reported abundance value in proteome data. If the protein

abundance value was missing, then the original abundance was used. Whether a specific phosphopetide is normalized or not is indicated in S5 File under the "Normalized" column.

CLOCK O-GlcNAcylation detection

Around 300-400mg liver tissue was used for CLOCK O-GlcNAcylation detection. The protocol was adapted from Yoshitane et al. [108] and Cao et al. [109] with the following modifications. Crude nuclei were extracted as described above with modified Buffer A (10mM HEPES pH7.9, 10mM KCl, 0.1mM EDTA, 1mM DTT, 1mM PMSF, 50mM NaF, 100μM PUGNAc, and Roche EDTA-free protease inhibitor cocktail). Nuclear proteins were extracted using nuclear extraction buffer (NEB) (20mM HEPES pH7.9, 10% Glycerol, 400mM NaCl, 1% Triton X-100, 0.1% sodium deoxycholate, 1mM EDTA, 5mM $MgCl_2$, 1mM DTT, 0.5mM PMSF, 10mM NaF, Roche PhoSTOP, 100μM PUGNAc, and Roche EDTA-free protease inhibitor cocktail) by rotating at 4°C for 30 mins. The soluble and non-soluble nuclear fractions were separated by centrifuging at 16000g for 15 mins. Prior to immunoprecipitation, samples were diluted using buffer D (20mM HEPES, pH7.9, 10% Glycerol, 1mM EDTA, 1mM DTT, 0.5mM PMSF, 10mM NaF, Roche PhosSTOP, 100μM PUGNAc, and Roche EDTA-free protease inhibitor cocktail) at 3:5 (V_{NEB}: V_D). Immunoprecipitation was performed using 4μl α-CLOCK (Cat# ab3517, Abcam, Boston, MA) in combination with 20 μl gammabind Sepharose beads (GE HealthCare, Chicago, IL). 5μl of beads was collected for detection of CLOCK protein, and Western blot was performed with α-CLOCK (1:3000).

For O-GlcNAcylation detection, the rest of the beads was washed twice with wash buffer (20mM HEPES, pH7.9, 10% Glycerol, 150mM NaCl, 1mM EDTA, 1mM DTT, 2mM $MgCl_2$, 0.5mM PMSF, 10mM NaF, 100μM PUGNAc, and Roche EDTA-free protease inhibitor cocktail) and twice with reaction buffer (20mM HEPES pH7.9, 50mM NaCl, 25mM NaF, 0.5mM PMSF, 5mM $MnCl_2$, 1μM PUGNAc, and Roche EDTA-free protease inhibitor cocktail). After washing, 16μl of reaction buffer, 2μl of GalT1(Y289L) and 2μl of 0.5mM UDP-GalNAz were added and the mixture incubated at 4°C overnight. On the second day, the beads were washed twice with the reaction buffer to remove excess UDP-GalNAz, and 37.5μl 1% SDS with 20mM HEPES pH7.9 was added to the resin. Finally, biotinylation was performed using a biotinylation buffer (1xPBS, 100μM biotin alkyne, 2mM sodium ascorbate, 100μM Tris (benzyltriazolylmethyl) amine, and 1mM $CuSO_4$). To prepare for Western blot, samples were precipitated using the chloroform-

methanol method and dissolved in 50µl 1% SDS with 20mM HEPES pH7.9. O-GlcNAcylated proteins were detected using α-streptavidin-HRP (Cell Signaling Technologies) (1:5000).

Bioinformatic and statistical analysis

For O-GlcNAcomics, peptide count was first normalized to the input protein amount for IP with streptavidin beads. Similar to the TMT phosphoproteomics analysis, the O-GlcNAcylated protein peptide counts were further normalized to their protein level obtained from the TMT-MS analysis performed in parallel using the same samples, if the protein was detected [107]. If the protein expression level was not sufficiently resolved, the original peptide count was maintained [107]. Whether a specific O-GlcNAc protein is normalized or not is indicated in S5 File under the "Normalized" column. Due to the batch effect observed in our dataset, we split the 4 biological replicates into 2 batches (2 biological replicates in each of the 2 batches) for the following analysis. Labeled samples and unlabeled samples were compared by Significance Analysis of INTeractome (SAINT) to identify high confident O-GlcNAc proteins [62].

Rhythmicity, phase and period length of O-GlcNAc proteins and phosphopeptides were determined using Rhythmic Analysis Incorporating Nonparametric (RAIN) [60]. For the O-GlcNAcome, the rhythmically O-GlcNAcylated proteins detected in both batches were combined together with the batch numbers indicated in the "RAIN test for O-GlcNAcome" sheet of S2 File. For kinase analysis, the kinase motifs on phosphopeptides were enriched using PTMphinder [67] and the enriched motifs were then fed into group-based phosphorylation site predicting and scoring (GPS) 5.0 to predict the kinases [68]. We utilized the CORUM database [64] to identify protein complexes with rhythmic O-GlcNAcylation and/or phosphorylation on complex subunit(s). Spearman correlation was used to determine the correlation between rhythmic O-GlcNAcome versus rhythmic phosphoproteome on the same protein as well as the correlation between rhythmic O-GlcNAcome and phosphoproteome versus rhythmic target gene expression. RAIN, PTMphinder, protein complex analysis, Spearman correlation analysis were performed in R v4.2.2. The median levels of O-GlcNAcylation and UDP-GlcNAc in DRF and NRF groups were compared using Student's t test in GraphPad Prism 10.0 (GraphPad Software, La Jolla California USA), while the feeding amount between DRF and NRF was compared using Mann-Whitney test.

References

1. Bass JT. The circadian clock system's influence in health and disease. Genome Med. 2017;9: 94. doi:10.1186/s13073-017-0485-2

2. Patke A, Young MW, Axelrod S. Molecular mechanisms and physiological importance of circadian rhythms. Nat Rev Mol Cell Biol. 2020;21: 67–84. doi:10.1038/s41580-019-0179-2

3. Davis S, Mirick DK, Stevens RG. Night shift work, light at night, and risk of breast cancer. J Natl Cancer Inst. 2001;93: 1557–1562. doi:10.1093/jnci/93.20.1557

4. Fujino Y, Iso H, Tamakoshi A, Inaba Y, Koizumi A, Kubo T, et al. A prospective cohort study of shift work and risk of ischemic heart disease in Japanese male workers. Am J Epidemiol. 2006;164: 128–135. doi:10.1093/aje/kwj185

5. Gao Y, Gan T, Jiang L, Yu L, Tang D, Wang Y, et al. Association between shift work and risk of type 2 diabetes mellitus: a systematic review and dose-response meta-analysis of observational studies. Chronobiol Int. 2020;37: 29–46. doi:10.1080/07420528.2019.1683570

6. Roenneberg T, Merrow M. The Circadian Clock and Human Health. Curr Biol. 2016;26: R432-443. doi:10.1016/j.cub.2016.04.011

7. Takahashi JS. Transcriptional architecture of the mammalian circadian clock. Nat Rev Genet. 2017;18: 164–179. doi:10.1038/nrg.2016.150

8. Moore RY, Eichler VB. Loss of a circadian adrenal corticosterone rhythm following suprachiasmatic lesions in the rat. Brain Res. 1972;42: 201–206. doi:10.1016/0006-8993(72)90054-6

9. Stephan FK, Zucker I. Circadian rhythms in drinking behavior and locomotor activity of rats are eliminated by hypothalamic lesions. Proc Natl Acad Sci U S A. 1972;69: 1583–1586. doi:10.1073/pnas.69.6.1583

10. Schibler U, Gotic I, Saini C, Gos P, Curie T, Emmenegger Y, et al. Clock-Talk: Interactions between Central and Peripheral Circadian Oscillators in Mammals. Cold Spring Harb Symp Quant Biol. 2015;80: 223–232. doi:10.1101/sqb.2015.80.027490

11. Xin H, Deng F, Zhou M, Huang R, Ma X, Tian H, et al. A multi-tissue multi-omics analysis reveals distinct kineztics in entrainment of diurnal transcriptomes by inverted feeding. iScience. 2021;24: 102335. doi:10.1016/j.isci.2021.102335

12. Koronowski KB, Kinouchi K, Welz P-S, Smith JG, Zinna VM, Shi J, et al. Defining the Independence of the Liver Circadian Clock. Cell. 2019;177: 1448-1462.e14. doi:10.1016/j.cell.2019.04.025

13. Reinke H, Asher G. Crosstalk between metabolism and circadian clocks. Nat Rev Mol Cell Biol. 2019;20: 227–241. doi:10.1038/s41580-018-0096-9

14. Stokkan KA, Yamazaki S, Tei H, Sakaki Y, Menaker M. Entrainment of the circadian clock in the liver by feeding. Science. 2001;291: 490–493. doi:10.1126/science.291.5503.490

15. Damiola F, Le Minh N, Preitner N, Kornmann B, Fleury-Olela F, Schibler U. Restricted feeding uncouples circadian oscillators in peripheral tissues from the central pacemaker in the suprachiasmatic nucleus. Genes Dev. 2000;14: 2950–2961. doi:10.1101/gad.183500

16. Panda S. Circadian physiology of metabolism. Science. 2016;354: 1008–1015. doi:10.1126/science.aah4967

17. Lamia KA, Sachdeva UM, DiTacchio L, Williams EC, Alvarez JG, Egan DF, et al. AMPK regulates the circadian clock by cryptochrome phosphorylation and degradation. Science. 2009;326: 437–440. doi:10.1126/science.1172156

18. Asher G, Reinke H, Altmeyer M, Gutierrez-Arcelus M, Hottiger MO, Schibler U. Poly(ADP-ribose) polymerase 1 participates in the phase entrainment of circadian clocks to feeding. Cell. 2010;142: 943–953. doi:10.1016/j.cell.2010.08.016

19. Weger BD, Gobet C, David FPA, Atger F, Martin E, Phillips NE, et al. Systematic analysis of differential rhythmic liver gene expression mediated by the circadian clock and feeding rhythms. Proc Natl Acad Sci USA. 2021;118: e2015803118. doi:10.1073/pnas.2015803118

20. Vollmers C, Gill S, DiTacchio L, Pulivarthy SR, Le HD, Panda S. Time of feeding and the intrinsic circadian clock drive rhythms in hepatic gene expression. Proc Natl Acad Sci U S A. 2009;106: 21453–21458. doi:10.1073/pnas.0909591106

21. Greenwell BJ, Trott AJ, Beytebiere JR, Pao S, Bosley A, Beach E, et al. Rhythmic Food Intake Drives Rhythmic Gene Expression More Potently than the Hepatic Circadian Clock in Mice. Cell Reports. 2019;27: 649-657.e5. doi:10.1016/j.celrep.2019.03.064

22. Atger F, Gobet C, Marquis J, Martin E, Wang J, Weger B, et al. Circadian and feeding rhythms differentially affect rhythmic mRNA transcription and translation in mouse liver. Proc Natl Acad Sci U S A. 2015;112: E6579-6588. doi:10.1073/pnas.1515308112

23. Chatham JC, Zhang J, Wende AR. Role of *O* -linked *N* -acetylglucosamine protein modification in cellular (patho)physiology. Physiological Reviews. 2021;101: 427–493. doi:10.1152/physrev.00043.2019

24. Wulff-Fuentes E, Berendt RR, Massman L, Danner L, Malard F, Vora J, et al. The human O-GlcNAcome database and meta-analysis. Sci Data. 2021;8: 25. doi:10.1038/s41597-021-00810-4

25. Ma J, Hou C, Wu C. Demystifying the O-GlcNAc Code: A Systems View. Chem Rev. 2022; acs.chemrev.1c01006. doi:10.1021/acs.chemrev.1c01006

26. Wang Y, Fang X, Wang S, Wang B, Chu F, Tian Z, et al. The role of O-GlcNAcylation in innate immunity and inflammation. J Mol Cell Biol. 2023;14: mjac065. doi:10.1093/jmcb/mjac065

27. Liu X, Chiu JC. Nutrient-sensitive protein O-GlcNAcylation shapes daily biological rhythms. Open Biology. 2022;12: 220215. doi:10.1098/rsob.220215

28. Liu X, Cai YD, Chiu JC. Regulation of protein O-GlcNAcylation by circadian, metabolic, and cellular signals. J Biol Chem. 2023;300: 105616. doi:10.1016/j.jbc.2023.105616

29. Durgan DJ, Pat BM, Laczy B, Bradley JA, Tsai J-Y, Grenett MH, et al. O-GlcNAcylation, Novel Post-Translational Modification Linking Myocardial Metabolism and Cardiomyocyte Circadian Clock*. Journal of Biological Chemistry. 2011;286: 44606–44619. doi:10.1074/jbc.M111.278903

30. Liu X, Blaženović I, Contreras AJ, Pham TM, Tabuloc CA, Li YH, et al. Hexosamine biosynthetic pathway and O-GlcNAc-processing enzymes regulate daily rhythms in protein O-GlcNAcylation. Nat Commun. 2021;12: 4173. doi:10.1038/s41467-021-24301-7

31. Hart GW. Nutrient regulation of signaling and transcription. Journal of Biological Chemistry. 2019;294: 2211–2231. doi:10.1074/jbc.AW119.003226

32. Li M-D, Ruan H-B, Hughes ME, Lee J-S, Singh JP, Jones SP, et al. O-GlcNAc Signaling Entrains the Circadian Clock by Inhibiting BMAL1/CLOCK Ubiquitination. Cell Metabolism. 2013;17: 303–310. doi:10.1016/j.cmet.2012.12.015

33. Han I, Kudlow JE. Reduced O glycosylation of Sp1 is associated with increased proteasome susceptibility. Mol Cell Biol. 1997;17: 2550–2558. doi:10.1128/MCB.17.5.2550

34. Zhang F, Su K, Yang X, Bowe DB, Paterson AJ, Kudlow JE. O-GlcNAc modification is an endogenous inhibitor of the proteasome. Cell. 2003;115: 715–725. doi:10.1016/s0092-8674(03)00974-7

35. Yang A-Q, Li D, Chi L, Ye X-S. Validation, Identification, and Biological Consequences of the Site-specific O-GlcNAcylation Dynamics of Carbohydrate-responsive Element-binding Protein (ChREBP). Mol Cell Proteomics. 2017;16: 1233–1243. doi:10.1074/mcp.M116.061416

36. Issad T, Kuo M. O-GlcNAc modification of transcription factors, glucose sensing and glucotoxicity. Trends Endocrinol Metab. 2008;19: 380–389. doi:10.1016/j.tem.2008.09.001

37. Hardivillé S, Banerjee PS, Selen Alpergin ES, Smith DM, Han G, Ma J, et al. TATA-Box Binding Protein O-GlcNAcylation at T114 Regulates Formation of the B-TFIID Complex and Is Critical for Metabolic Gene Regulation. Mol Cell. 2020;77: 1143-1152.e7. doi:10.1016/j.molcel.2019.11.022

38. Noach N, Segev Y, Levi I, Segal S, Priel E. Modification of topoisomerase I activity by glucose and by O-GlcNAcylation of the enzyme protein. Glycobiology. 2007;17: 1357–1364. doi:10.1093/glycob/cwm105

39. Ranuncolo SM, Ghosh S, Hanover JA, Hart GW, Lewis BA. Evidence of the Involvement of O-GlcNAc-modified Human RNA Polymerase II CTD in Transcription in Vitro and in Vivo. Journal of Biological Chemistry. 2012;287: 23549–23561. doi:10.1074/jbc.M111.330910

40. Lewis BA, Burlingame AL, Myers SA. Human RNA Polymerase II Promoter Recruitment in Vitro Is Regulated by O-Linked N-Acetylglucosaminyltransferase (OGT). J Biol Chem. 2016;291: 14056–14061. doi:10.1074/jbc.M115.684365

41. Shi F-T, Kim H, Lu W, He Q, Liu D, Goodell MA, et al. Ten-eleven translocation 1 (Tet1) is regulated by O-linked N-acetylglucosamine transferase (Ogt) for target gene repression in mouse embryonic stem cells. J Biol Chem. 2013;288: 20776–20784. doi:10.1074/jbc.M113.460386

42. Li H-J, Wang Y, Li B-X, Yang Y, Guan F, Pang X-C, et al. Roles of ten-eleven translocation family proteins and their O-linked β-N-acetylglucosaminylated forms in cancer development. Oncol Lett. 2021;21: 1. doi:10.3892/ol.2020.12262

43. Vella P, Scelfo A, Jammula S, Chiacchiera F, Williams K, Cuomo A, et al. Tet Proteins Connect the O-Linked N-acetylglucosamine Transferase Ogt to Chromatin in Embryonic Stem Cells. Molecular Cell. 2013;49: 645–656. doi:10.1016/j.molcel.2012.12.019

44. Zhang Q, Liu X, Gao W, Li P, Hou J, Li J, et al. Differential regulation of the ten-eleven translocation (TET) family of dioxygenases by O-linked β-N-acetylglucosamine transferase (OGT). J Biol Chem. 2014;289: 5986–5996. doi:10.1074/jbc.M113.524140

45. Leturcq M, Lefebvre T, Vercoutter-Edouart A-S. O-GlcNAcylation and chromatin remodeling in mammals: an up-to-date overview. Biochem Soc Trans. 2017;45: 323–338. doi:10.1042/BST20160388

46. Zhang S, Roche K, Nasheuer H-P, Lowndes NF. Modification of histones by sugar β-N-acetylglucosamine (GlcNAc) occurs on multiple residues, including histone H3 serine 10, and is cell cycle-regulated. J Biol Chem. 2011;286: 37483–37495. doi:10.1074/jbc.M111.284885

47. Fong JJ, Nguyen BL, Bridger R, Medrano EE, Wells L, Pan S, et al. β-N-Acetylglucosamine (O-GlcNAc) Is a Novel Regulator of Mitosis-specific Phosphorylations on Histone H3. Journal of Biological Chemistry. 2012;287: 12195–12203. doi:10.1074/jbc.M111.315804

48. Wang P, Peng C, Liu X, Liu H, Chen Y, Zheng L, et al. OGT mediated histone H2B S112 GlcNAcylation regulates DNA damage response. J Genet Genomics. 2015;42: 467–475. doi:10.1016/j.jgg.2015.07.002

49. Dehennaut V, Leprince D, Lefebvre T. O-GlcNAcylation, an Epigenetic Mark. Focus on the Histone Code, TET Family Proteins, and Polycomb Group Proteins. Front Endocrinol (Lausanne). 2014;5: 155. doi:10.3389/fendo.2014.00155

50. Zhao M-J, Yao X, Wei P, Zhao C, Cheng M, Zhang D, et al. O-GlcNAcylation of TDP-43 suppresses proteinopathies and promotes TDP-43's mRNA splicing activity. EMBO Rep. 2021;22: e51649. doi:10.15252/embr.202051649

51. Tan W, Jiang P, Zhang W, Hu Z, Lin S, Chen L, et al. Posttranscriptional regulation of de novo lipogenesis by glucose-induced O-GlcNAcylation. Molecular Cell. 2021;81: 1890-1904.e7. doi:10.1016/j.molcel.2021.02.009

52. Tan Z-W, Fei G, Paulo JA, Bellaousov S, Martin SES, Duveau DY, et al. O-GlcNAc regulates gene expression by controlling detained intron splicing. Nucleic Acids Res. 2020;48: 5656–5669. doi:10.1093/nar/gkaa263

53. Laarse SAM, Leney AC, Heck AJR. Crosstalk between phosphorylation and O-Glc NA cylation: friend or foe. FEBS J. 2018;285: 3152–3167. doi:10.1111/febs.14491

54. Kaasik K, Kivimäe S, Allen JJ, Chalkley RJ, Huang Y, Baer K, et al. Glucose Sensor O-GlcNAcylation Coordinates with Phosphorylation to Regulate Circadian Clock. Cell Metabolism. 2013;17: 291–302. doi:10.1016/j.cmet.2012.12.017

55. Wang Y, Song L, Liu M, Ge R, Zhou Q, Liu W, et al. A proteomics landscape of circadian clock in mouse liver. Nat Commun. 2018;9: 1553. doi:10.1038/s41467-018-03898-2

56. Wang J, Mauvoisin D, Martin E, Atger F, Galindo AN, Dayon L, et al. Nuclear Proteomics Uncovers Diurnal Regulatory Landscapes in Mouse Liver. Cell Metabolism. 2017;25: 102–117. doi:10.1016/j.cmet.2016.10.003

57. Robles MS, Humphrey SJ, Mann M. Phosphorylation Is a Central Mechanism for Circadian Control of Metabolism and Physiology. Cell Metabolism. 2017;25: 118–127. doi:10.1016/j.cmet.2016.10.004

58. Huang R, Chen J, Zhou M, Xin H, Lam SM, Jiang X, et al. Multi-omics profiling reveals rhythmic liver function shaped by meal timing. Nat Commun. 2023;14: 6086. doi:10.1038/s41467-023-41759-9

59. Thompson JW, Griffin ME, Hsieh-Wilson LC. Methods for the Detection, Study, and Dynamic Profiling of O-GlcNAc Glycosylation. Methods Enzymol. 2018;598: 101–135. doi:10.1016/bs.mie.2017.06.009

60. Thaben PF, Westermark PO. Detecting Rhythms in Time Series with RAIN. J Biol Rhythms. 2014;29: 391–400. doi:10.1177/0748730414553029

61. Phua S-X, Lim K-P, Goh WW-B. Perspectives for better batch effect correction in mass-spectrometry-based proteomics. Comput Struct Biotechnol J. 2022;20: 4369–4375. doi:10.1016/j.csbj.2022.08.022

62. Choi H, Larsen B, Lin Z-Y, Breitkreutz A, Mellacheruvu D, Fermin D, et al. SAINT: probabilistic scoring of affinity purification-mass spectrometry data. Nat Methods. 2011;8: 70–73. doi:10.1038/nmeth.1541

63. Burt RA, Alghusen IM, John Ephrame S, Villar MT, Artigues A, Slawson C. Mapping the O-GlcNAc Modified Proteome: Applications for Health and Disease. Front Mol Biosci. 2022;9: 920727. doi:10.3389/fmolb.2022.920727

64. Tsitsiridis G, Steinkamp R, Giurgiu M, Brauner B, Fobo, Frishman G, et al. CORUM: the comprehensive resource of mammalian protein complexes-2022. Nucleic acids research. 2023;51. doi:10.1093/nar/gkac1015

65. Yao H, Li A, Wang M. Systematic Analysis and Prediction of *In Situ* Cross Talk of O-GlcNAcylation and Phosphorylation. BioMed Research International. 2015;2015: 1–12. doi:10.1155/2015/279823

66. Leney AC, El Atmioui D, Wu W, Ovaa H, Heck AJR. Elucidating crosstalk mechanisms between phosphorylation and O-GlcNAcylation. Proc Natl Acad Sci USA. 2017;114. doi:10.1073/pnas.1620529114

67. Wozniak JM, Gonzalez DJ. PTMphinder: an R package for PTM site localization and motif extraction from proteomic datasets. PeerJ. 2019;7: e7046. doi:10.7717/peerj.7046

68. Wang C, Xu H, Lin S, Deng W, Zhou J, Zhang Y, et al. GPS 5.0: An Update on the Prediction of Kinase-specific Phosphorylation Sites in Proteins. Genomics Proteomics Bioinformatics. 2020;18: 72–80. doi:10.1016/j.gpb.2020.01.001

69. Eckel-Mahan KL, Phan T, Han S, Wang H, Chan GC-K, Scheiner ZS, et al. Circadian oscillation of hippocampal MAPK activity and cAMP: implications for memory persistence. Nat Neurosci. 2008;11: 1074–1082. doi:10.1038/nn.2174

70. Agostino PV, Ferreyra GA, Murad AD, Watanabe Y, Golombek DA. Diurnal, circadian and photic regulation of calcium/calmodulin-dependent kinase II and neuronal nitric oxide synthase in the hamster suprachiasmatic nuclei. Neurochem Int. 2004;44: 617–625. doi:10.1016/j.neuint.2003.09.005

71. Butcher GQ, Lee B, Hsieh F, Obrietan K. Light- and clock-dependent regulation of ribosomal S6 kinase activity in the suprachiasmatic nucleus. Eur J Neurosci. 2004;19: 907–915. doi:10.1111/j.0953-816x.2004.03155.x

72. Brenna A, Albrecht U. Phosphorylation and Circadian Molecular Timing. Front Physiol. 2020;11: 612510. doi:10.3389/fphys.2020.612510

73. Spengler ML, Kuropatwinski KK, Schumer M, Antoch MP. A serine cluster mediates BMAL1-dependent CLOCK phosphorylation and degradation. Cell Cycle. 2009;8: 4138–4146. doi:10.4161/cc.8.24.10273

74. Hansen K, Farkas T, Lukas J, Holm K, Rönnstrand L, Bartek J. Phosphorylation-dependent and -independent functions of p130 cooperate to evoke a sustained G1 block. EMBO J. 2001;20: 422–432. doi:10.1093/emboj/20.3.422

75. Farkas T, Hansen K, Holm K, Lukas J, Bartek J. Distinct phosphorylation events regulate p130- and p107-mediated repression of E2F-4. J Biol Chem. 2002;277: 26741–26752. doi:10.1074/jbc.M200381200

76. Beurel E, Grieco SF, Jope RS. Glycogen synthase kinase-3 (GSK3): regulation, actions, and diseases. Pharmacol Ther. 2015;0: 114–131. doi:10.1016/j.pharmthera.2014.11.016

77. Shi J, Sharif S, Ruijtenbeek R, Pieters RJ. Activity Based High-Throughput Screening for Novel O-GlcNAc Transferase Substrates Using a Dynamic Peptide Microarray. PLoS One. 2016;11: e0151085. doi:10.1371/journal.pone.0151085

78. Greco CM, Koronowski KB, Smith JG, Shi J, Kunderfranco P, Carriero R, et al. Integration of feeding behavior by the liver circadian clock reveals network dependency of metabolic rhythms. Sci Adv. 2021;7: eabi7828. doi:10.1126/sciadv.abi7828

79. Ren B, Cam H, Takahashi Y, Volkert T, Terragni J, Young RA, et al. E2F integrates cell cycle progression with DNA repair, replication, and G(2)/M checkpoints. Genes Dev. 2002;16: 245–256. doi:10.1101/gad.949802

80. Lee B-K, Bhinge AA, Iyer VR. Wide-ranging functions of E2F4 in transcriptional activation and repression revealed by genome-wide analysis. Nucleic Acids Res. 2011;39: 3558–3573. doi:10.1093/nar/gkq1313

81. Liska O, Bohár B, Hidas A, Korcsmáros T, Papp B, Fazekas D, et al. TFLink: an integrated gateway to access transcription factor-target gene interactions for multiple species. Database (Oxford). 2022;2022: baac083. doi:10.1093/database/baac083

82. Mendoza-Viveros L, Bouchard-Cannon P, Hegazi S, Cheng AH, Pastore S, Cheng H-YM. Molecular modulators of the circadian clock: lessons from flies and mice. Cell Mol Life Sci. 2017;74: 1035–1059. doi:10.1007/s00018-016-2378-8

83. Cramer P. Organization and regulation of gene transcription. Nature. 2019;573: 45–54. doi:10.1038/s41586-019-1517-4

84. Cruise TM, Kotlo K, Malovic E, Pandey SC. Advances in DNA, histone, and RNA methylation mechanisms in the pathophysiology of alcohol use disorder. Adv Drug Alcohol Res. 2023;3: 10871. doi:10.3389/adar.2023.10871

85. Nosella ML, Tereshchenko M, Pritišanac I, Chong PA, Toretsky JA, Lee HO, et al. O-Linked-N-Acetylglucosaminylation of the RNA-Binding Protein EWS N-Terminal Low Complexity Region Reduces Phase Separation and Enhances Condensate Dynamics. J Am Chem Soc. 2021;143: 11520–11534. doi:10.1021/jacs.1c04194

86. Shin H, Cha H-J, Na K, Lee MJ, Cho J-Y, Kim C-Y, et al. O-GlcNAcylation of the Tumor Suppressor FOXO3 Triggers Aberrant Cancer Cell Growth. Cancer Res. 2018;78: 1214–1224. doi:10.1158/0008-5472.CAN-17-3512

87. Li Z, Fu B, Wei A, Wu Y, Huang M, Zhang E, et al. d-Glucosamine induces circadian phase delay by promoting BMAL1 degradation through AMPK/mTOR pathway. Life Sci. 2023;325: 121765. doi:10.1016/j.lfs.2023.121765

88. Crosby P, Hamnett R, Putker M, Hoyle NP, Reed M, Karam CJ, et al. Insulin/IGF-1 Drives PERIOD Synthesis to Entrain Circadian Rhythms with Feeding Time. Cell. 2019;177: 896-909.e20. doi:10.1016/j.cell.2019.02.017

89. Xu C, Pan X, Wang D, Guan Y, Yang W, Chen X, et al. O-GlcNAcylation of Raptor transduces glucose signals to mTORC1. Mol Cell. 2023;83: 3027-3040.e11. doi:10.1016/j.molcel.2023.07.011

90. Luo B, Parker GJ, Cooksey RC, Soesanto Y, Evans M, Jones D, et al. Chronic hexosamine flux stimulates fatty acid oxidation by activating AMP-activated protein kinase in adipocytes. J Biol Chem. 2007;282: 7172–7180. doi:10.1074/jbc.M607362200

91. Bullen JW, Balsbaugh JL, Chanda D, Shabanowitz J, Hunt DF, Neumann D, et al. Cross-talk between Two Essential Nutrient-sensitive Enzymes. Journal of Biological Chemistry. 2014;289: 10592–10606. doi:10.1074/jbc.M113.523068

92. Vosseller K, Wells L, Lane MD, Hart GW. Elevated nucleocytoplasmic glycosylation by O-GlcNAc results in insulin resistance associated with defects in Akt activation in 3T3-L1 adipocytes. Proc Natl Acad Sci U S A. 2002;99: 5313–5318. doi:10.1073/pnas.072072399

93. Makishima M, Okamoto AY, Repa JJ, Tu H, Learned RM, Luk A, et al. Identification of a nuclear receptor for bile acids. Science. 1999;284: 1362–1365. doi:10.1126/science.284.5418.1362

94. Ouyang Y, Wu Q, Li J, Sun S, Sun S. S-adenosylmethionine: A metabolite critical to the regulation of autophagy. Cell Prolif. 2020;53: e12891. doi:10.1111/cpr.12891

95. Oyama Y, Iwasaka H, Koga H, Shingu C, Matsumoto S, Noguchi T. Uncoupling of peripheral and master clock gene rhythms by reversed feeding leads to an exacerbated inflammatory response after polymicrobial sepsis in mice. Shock. 2014;41: 214–221. doi:10.1097/SHK.0000000000000094

96. Nagata T, Redman RS, Lakshman R. Isolation of intact nuclei of high purity from mouse liver. Anal Biochem. 2010;398: 178–184. doi:10.1016/j.ab.2009.11.017

97. Khidekel N, Arndt S, Lamarre-Vincent N, Lippert A, Poulin-Kerstien KG, Ramakrishnan B, et al. A chemoenzymatic approach toward the rapid and sensitive detection of O-GlcNAc posttranslational modifications. J Am Chem Soc. 2003;125: 16162–16163. doi:10.1021/ja038545r

98. Ramakrishnan B, Qasba PK. Structure-based design of beta 1,4-galactosyltransferase I (beta 4Gal-T1) with equally efficient N-acetylgalactosaminyltransferase activity: point mutation broadens beta 4Gal-T1 donor specificity. J Biol Chem. 2002;277: 20833–20839. doi:10.1074/jbc.M111183200

99. Fiehn O. Metabolomics by Gas Chromatography-Mass Spectrometry: Combined Targeted and Untargeted Profiling. Curr Protoc Mol Biol. 2016;114: 30.4.1-30.4.32. doi:10.1002/0471142727.mb3004s114

100. Tsugawa H, Cajka T, Kind T, Ma Y, Higgins B, Ikeda K, et al. MS-DIAL: data-independent MS/MS deconvolution for comprehensive metabolome analysis. Nat Methods. 2015;12: 523–526. doi:10.1038/nmeth.3393

101. Mohammed H, Taylor C, Brown GD, Papachristou EK, Carroll JS, D'Santos CS. Rapid immunoprecipitation mass spectrometry of endogenous proteins (RIME) for analysis of chromatin complexes. Nat Protoc. 2016;11: 316–326. doi:10.1038/nprot.2016.020

102. Sharma S, Yang J, Grudzien-Nogalska E, Shivas J, Kwan KY, Kiledjian M. Xrn1 is a deNADding enzyme modulating mitochondrial NAD-capped RNA. Nat Commun. 2022;13: 889. doi:10.1038/s41467-022-28555-7

103. Craig R, Beavis RC. TANDEM: matching proteins with tandem mass spectra. Bioinformatics. 2004;20: 1466–1467. doi:10.1093/bioinformatics/bth092

104. Gupta N, Bandeira N, Keich U, Pevzner PA. Target-decoy approach and false discovery rate: when things may go wrong. J Am Soc Mass Spectrom. 2011;22: 1111–1120. doi:10.1007/s13361-011-0139-3

105. Li J, Cai Z, Bomgarden RD, Pike I, Kuhn K, Rogers JC, et al. TMTpro-18plex: The Expanded and Complete Set of TMTpro Reagents for Sample Multiplexing. J Proteome Res. 2021;20: 2964–2972. doi:10.1021/acs.jproteome.1c00168

106. Mertins P, Qiao JW, Patel J, Udeshi ND, Clauser KR, Mani DR, et al. Integrated proteomic analysis of post-translational modifications by serial enrichment. Nat Methods. 2013;10: 634–637. doi:10.1038/nmeth.2518

107. Li J, Paulo JA, Nusinow DP, Huttlin EL, Gygi SP. Investigation of Proteomic and Phosphoproteomic Responses to Signaling Network Perturbations Reveals Functional Pathway Organizations in Yeast. Cell Rep. 2019;29: 2092-2104.e4. doi:10.1016/j.celrep.2019.10.034

108. Yoshitane H, Takao T, Satomi Y, Du N-H, Okano T, Fukada Y. Roles of CLOCK phosphorylation in suppression of E-box-dependent transcription. Mol Cell Biol. 2009;29: 3675–3686. doi:10.1128/MCB.01864-08

109. Cao X, Yang Y, Selby C, Liu Z, Sancar A. Molecular mechanism of the repressive phase of the mammalian circadian clock. Proceedings of the National Academy of Sciences of the United States of America. 2021;118. doi:10.1073/pnas.2021174118

Acknowledgments: We would like to thank the West Coast Metabolomics Center at UC Davis for their technical support. This work is supported by National Institutes of Health grants R01 DK124068 and R56 DK124068 to J.C.C.

Author contributions: J.C.C., Y.K.X. and X.L. conceptualized and designed the study. J.C.C. acquired the funding. J.C.C., X.L. and Y.D.C. coordinated and supervised the investigation. X.L., Y.D.C., A.J.P.M., X.X., Y.L., H.Z. and C.Z. performed research and analyzed data. X.L., Y.D.C. and J.C.C. contributed to critical interpretation of the data. X.L., Y.D.C. and J.C.C. drafted the manuscript.

Competing Interests: The authors declare no competing interests.

Data Availability Statement: All data needed to evaluate the conclusions in the paper are present in the paper and/or the Supplementary Materials. The raw metabolomics dataset has been deposited in the open metabolomics database, Metabolomics Workbench (https://www.metabolomicsworkbench.org/), under accession no. [ST002952] and [ST002950]. The raw O-GlcNAcomics, TMT-phosphoproteomics and proteomics datasets have been deposited

into MassIVE repository (MSV000094417) (MassIVE: ftp://massive.ucsd.edu/v07/MSV000094417/). Data will be made public upon publication.

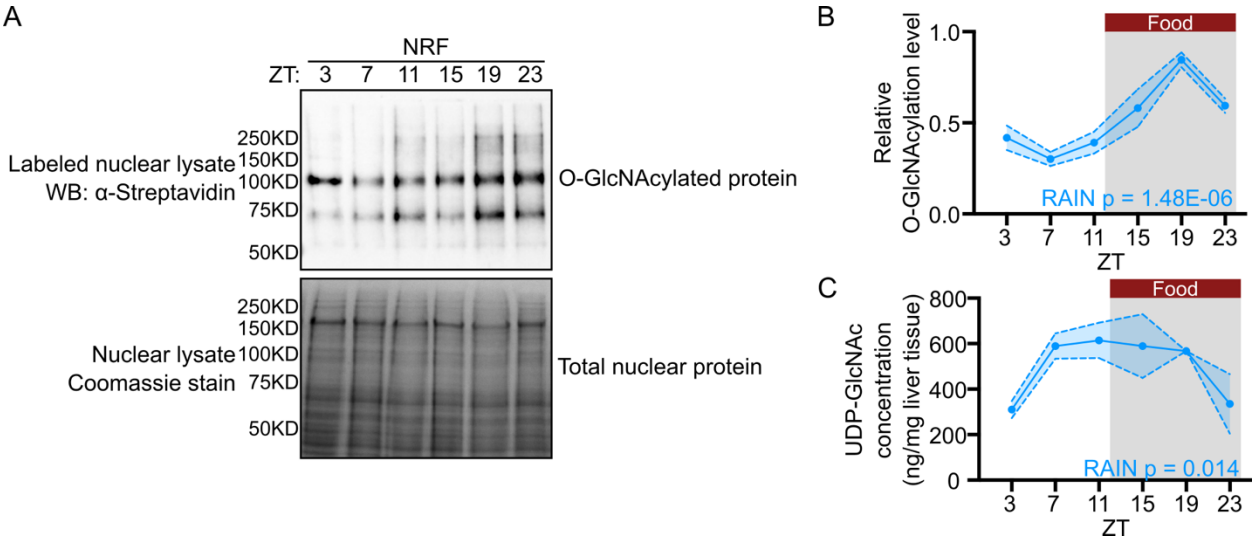

Fig 1. Protein O-GlcNAcylation exhibits daily rhythmicity in mouse liver nuclei

(A) Representative western blot showing the daily rhythm of nuclear protein O-GlcNAcylation in liver samples from mice fed during natural night feeding time (NRF). Total nuclear proteins were stained with Coomassie blue (bottom panel) and used for normalization. ZT, zeitgeber time (hr). ZT0 denotes lights-on time and ZT12 denotes lights-off time. **(B)** Quantification of protein O-GlcNAcylation signals in panel **(A)** (n = 3). α-streptavidin signal of the whole lane was quantified. **(C)** Daily rhythm of UDP-GlcNAc quantified using targeted metabolomics (n = 3). The grey shading in **(B)** and **(C)** illustrates the dark phase of the 24-hr day-night cycle. The red bars indicate when food was available. ZT: zeitgeber time (hr). Data are presented as mean ±SEM, and the blue shaded area represents SEM. P values indicate rhythmicity (RAIN).

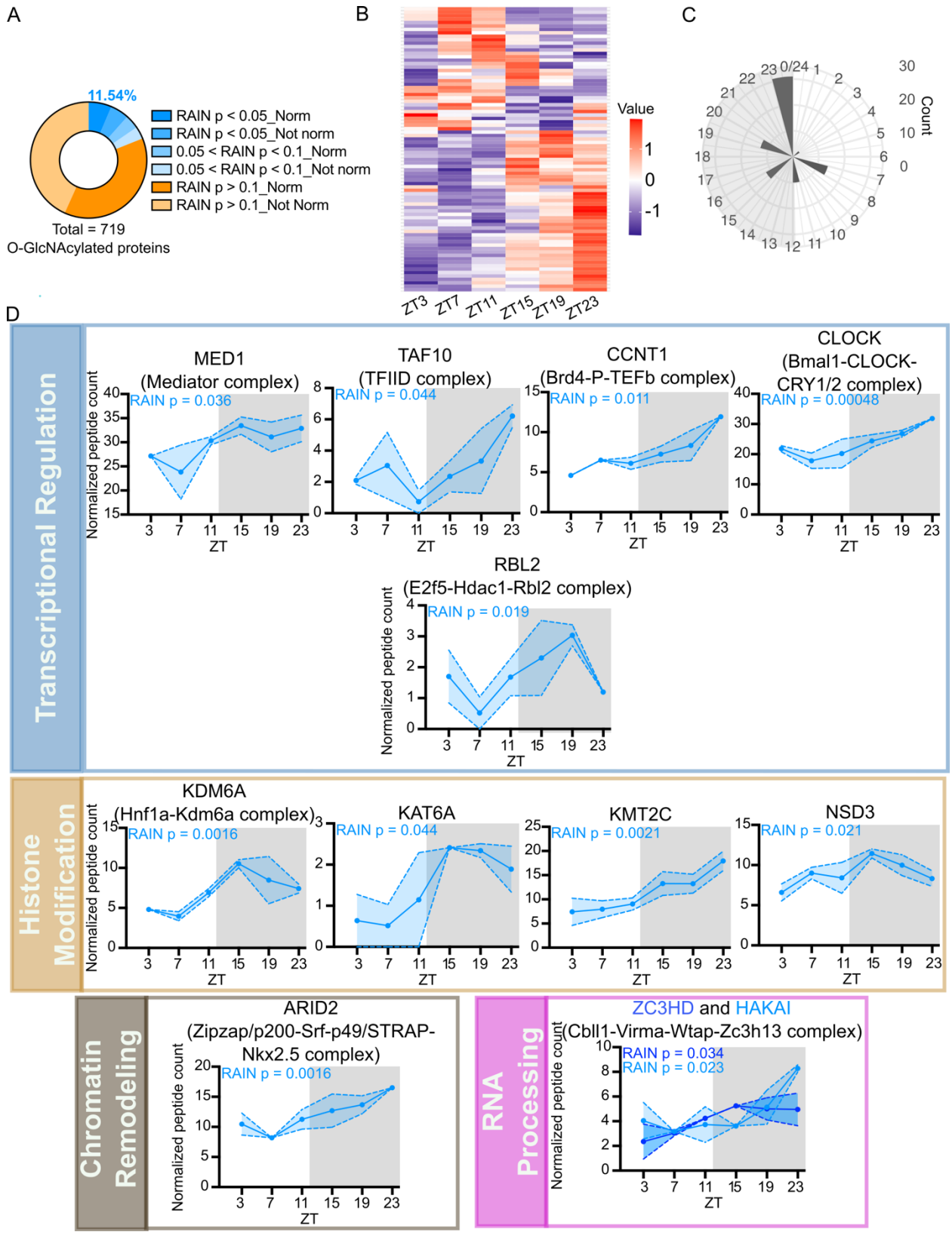
A
11.54%
RAIN p < 0.05_Norm
RAIN p < 0.05_Not norm
0.05 < RAIN p < 0.1_Norm
0.05 < RAIN p < 0.1_Not norm
RAIN p > 0.1_Norm
RAIN p > 0.1_Not Norm
Total = 719
O-GlcNAcylated proteins
B
Value
1
0
-1
ZT3
ZT7
ZT11
ZT15
ZT19
ZT23
C
Count
D
Transcriptional Regulation
MED1
(Mediator complex)
RAIN p = 0.036
TAF10
(TFIID complex)
RAIN p = 0.044
CCNT1
(Brd4-P-TEFb complex)
RAIN p = 0.011
CLOCK
(Bmal1-CLOCK-CRY1/2 complex)
RAIN p = 0.00048
RBL2
(E2f5-Hdac1-Rbl2 complex)
RAIN p = 0.019
Normalized peptide count
ZT
Histone Modification
KDM6A
(Hnf1a-Kdm6a complex)
RAIN p = 0.0016
KAT6A
RAIN p = 0.044
KMT2C
RAIN p = 0.0021
NSD3
RAIN p = 0.021
Chromatin Remodeling
ARID2
(Zipzap/p200-Srf-p49/STRAP-Nkx2.5 complex)
RAIN p = 0.0016
RNA Processing
ZC3HD and HAKAI
(Cbll1-Virma-Wtap-Zc3h13 complex)
RAIN p = 0.034
RAIN p = 0.023

Fig 2. Daily nuclear O-GlcNAcome of mouse liver from mice fed at natural night feeding time (NRF). (A) Pie chart showing the total number of O-GlcNAc proteins identified and the percentage of proteins with rhythmic O-GlcNAcylation determined by RAIN [60]. **(B)** Heat map showing the oscillation pattern of rhythmically O-GlcNAcylated proteins (n = 2). **(C)** Circular histogram showing the number of O-GlcNAcylated proteins peaking at each phase. The peak phase of O-GlcNAcylated proteins was calculated using RAIN. The gray shading illustrates the dark phase of a day-night cycle. **(D)** Rhythmically O-GlcNAcylated proteins were classified based on their known association in protein complexes, and the daily rhythmicity of the oscillating subunits were plotted. Multiple protein complexes were further classified and grouped according to their biological function as indicated on the left boxes. The gray shading illustrates the dark phase of a day-night cycle. Data are presented as mean ± SEM (n = 2), and the blue shading area around the curve represents ±SEM. P values indicates rhythmicity (RAIN).

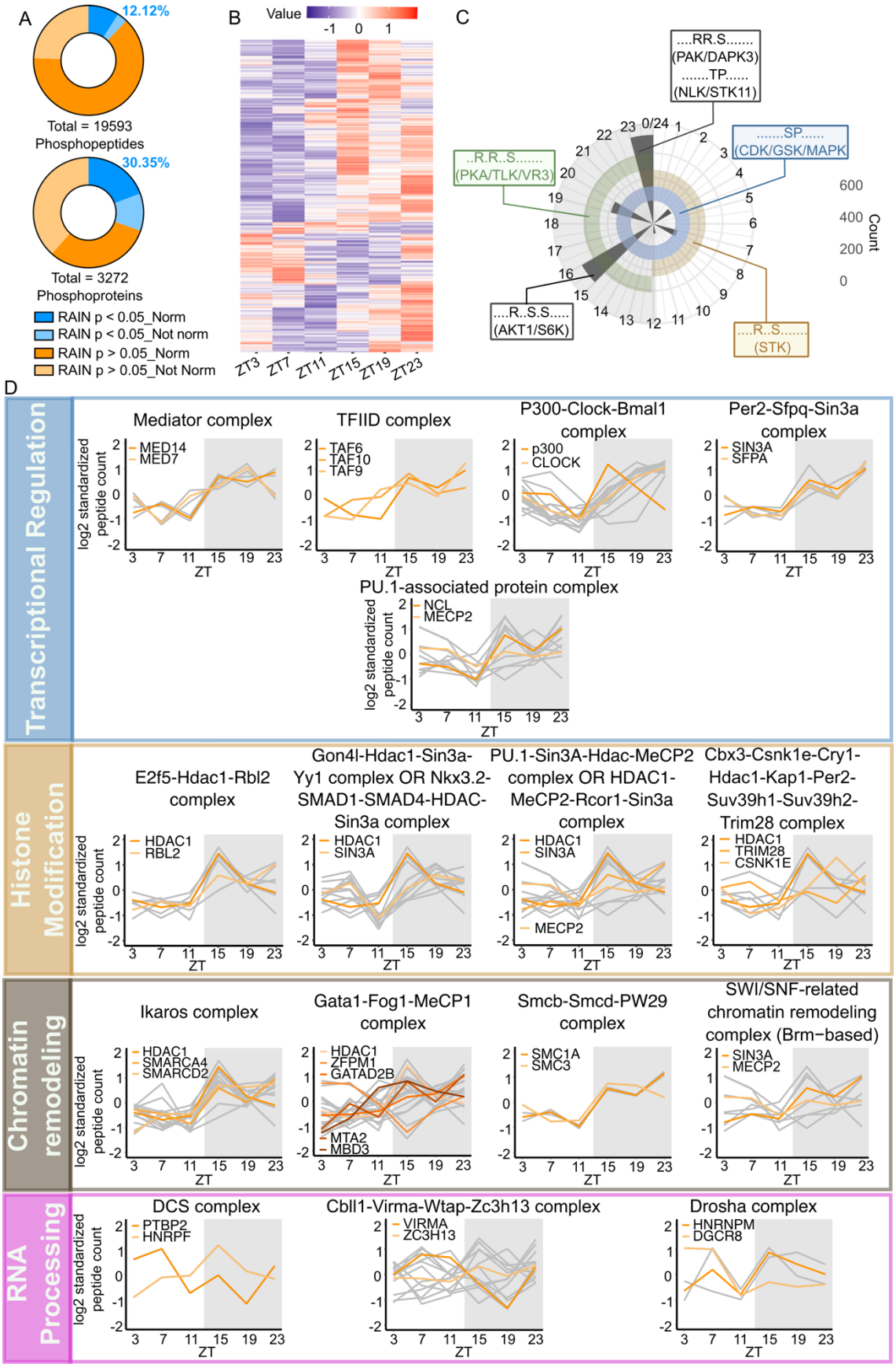
A
12.12%
Total = 19593
Phosphopeptides
30.35%
Total = 3272
Phosphoproteins
RAIN p < 0.05_Norm
RAIN p < 0.05_Not norm
RAIN p > 0.05_Norm
RAIN p > 0.05_Not Norm
B
Value
-1 0 1
ZT3 ZT7 ZT11 ZT15 ZT19 ZT23
C
....RR.S.....
(PAK/DAPK3)
.....TP.....
(NLK/STK11)
.....SP.....
(CDK/GSK/MAPK)
..R.R..S.....
(PKA/TLK/VR3)
....R..S.S.....
(AKT1/S6K)
....R..S.....
(STK)
Count
600
400
200
0
D
Transcriptional Regulation
Mediator complex
MED14
MED7
TFIID complex
TAF6
TAF10
TAF9
P300-Clock-Bmal1 complex
p300
CLOCK
Per2-Sfpq-Sin3a complex
SIN3A
SFPA
PU.1-associated protein complex
NCL
MECP2
log2 standardized peptide count
ZT
Histone Modification
E2f5-Hdac1-Rbl2 complex
HDAC1
RBL2
Gon4l-Hdac1-Sin3a-Yy1 complex OR Nkx3.2-SMAD1-SMAD4-HDAC-Sin3a complex
HDAC1
SIN3A
PU.1-Sin3A-Hdac-MeCP2 complex OR HDAC1-MeCP2-Rcor1-Sin3a complex
HDAC1
SIN3A
MECP2
Cbx3-Csnk1e-Cry1-Hdac1-Kap1-Per2-Suv39h1-Suv39h2-Trim28 complex
HDAC1
TRIM28
CSNK1E
Chromatin remodeling
Ikaros complex
HDAC1
SMARCA4
SMARCD2
Gata1-Fog1-MeCP1 complex
HDAC1
ZFPM1
GATAD2B
MTA2
MBD3
Smcb-Smcd-PW29 complex
SMC1A
SMC3
SWI/SNF-related chromatin remodeling complex (Brm−based)
SIN3A
MECP2
RNA Processing
DCS complex
PTBP2
HNRPF
Cbll1-Virma-Wtap-Zc3h13 complex
VIRMA
ZC3H13
Drosha complex
HNRNPM
DGCR8

Fig 3. Daily nuclear phosphoproteome of mouse liver from mice fed at NRF. (A) Pie chart showing the total number of phosphopeptides and phosphoproteins identified and the percentage of rhythmic phosphopeptides and proteins with rhythmic phosphorylation as determined by RAIN. **(B)** Heat map showing daily rhythmicity of phosphopeptides (n = 3). **(C)** Circular histogram showing the number of phosphopeptides peaking at each phase as determined by RAIN. The kinases that rhythmically phosphorylate the daily phosphoproteome were predicted based on the enriched peptide motifs in each peaking phase. The enriched peptide motifs and corresponding kinases were illustrated in the boxes. The color of boxes and shading corresponds to the phosphorylation motifs enriched from phosphopeptides peaking in the indicated phases. The gray shading illustrates the dark phase of a day-night cycle. **(D)** Rhythmically phosphorylated proteins were classified into protein complexes based on known association and function, and the subunits with daily rhythmicity in phosphorylation were plotted in graphs. The protein complexes were further classified and grouped according to their biological functions as indicated on the left boxes. The gray lines indicate the oscillation of each phosphopeptide, while the orange lines indicate the average phosphorylation pattern of each protein subunit. Each gray line represents the average of three biological replicates. The gray shading illustrates the dark phase of a day-night cycle.

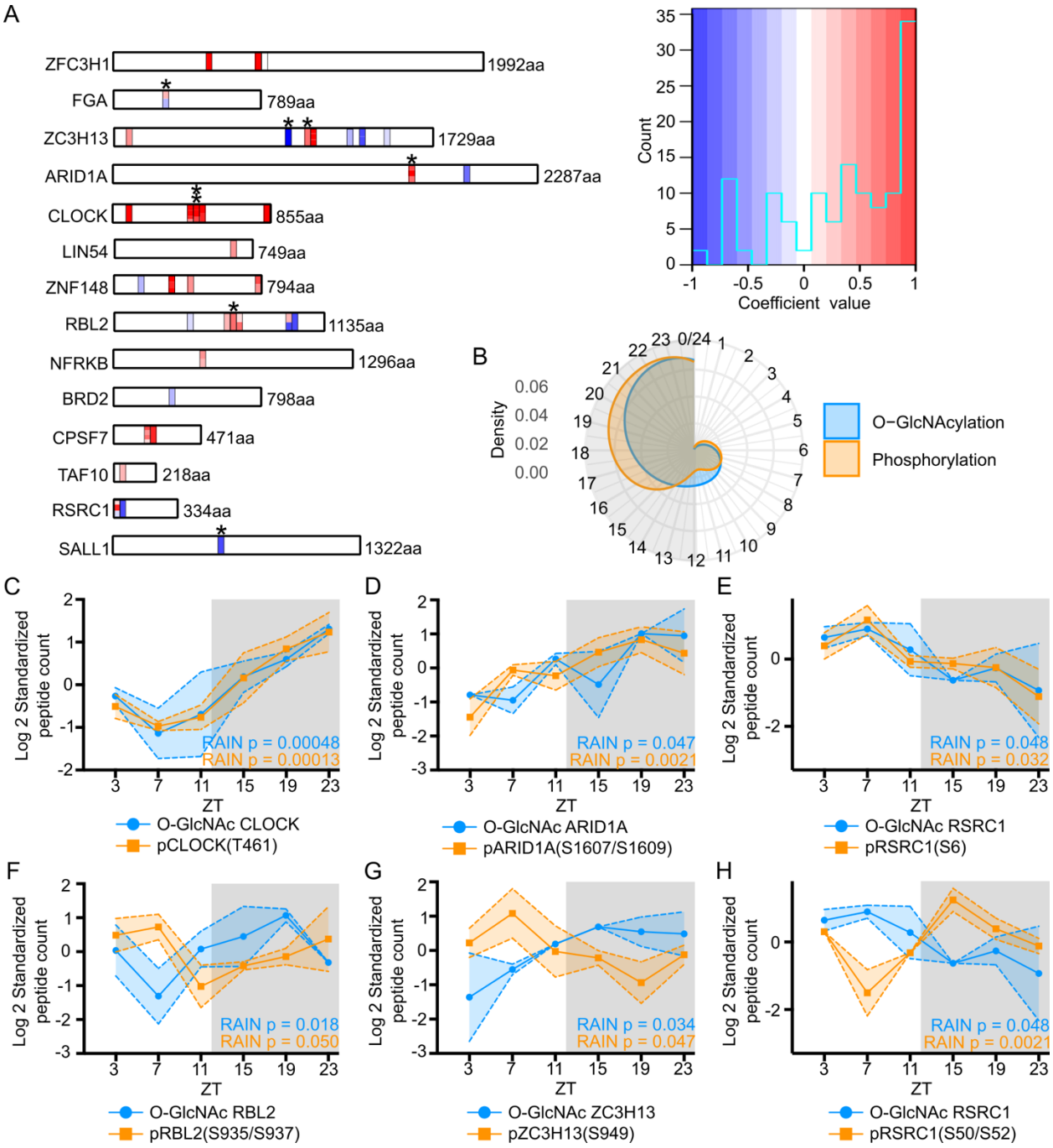

Fig 4. Interaction between the O-GlcNAcome and phosphoproteome over a day-night cycle. (A) Spearman correlation analysis showing the correlation between rhythmic O-GlcNAcylation and phosphorylation on each protein that exhibits daily rhythmicity of two PTMs. The color of the bars represents coefficient values as shown in the color scale on the right. The asterisks indicate the sites with potential O-GlcNAcylation and phosphorylation interplay motif. The color scale also includes a histogram showing the frequency of coefficient values between O-GlcNAcylation and

phosphorylation in proteins. **(B)** Circular density graphs showing the peak phase of O-GlcNAcylation and phosphorylation events on proteins that exhibit rhythmicity in both modifications. The gray shading illustrates the dark phase of a day-night cycle. **(C-H)** Examples of global O-GlcNAcylation compared to the temporal phosphorylation profiles on the same proteins. CLOCK and ARID1A represent proteins with in-phase rhythmic O-GlcNAcylation and phosphorylation **(C and D)**, while RBL2 and ZC3H13 represent proteins with out-of-phase rhythmic O-GlcNAcylation and phosphorylation **(F and G)**. RSRC1 represent proteins with both in-phase **(E)** and out-of-phase **(H)** rhythmic O-GlcNAcylation and phosphorylation. Data are presented as mean ± SEM (n = 3), and the shaded area around the curve represents SEM.

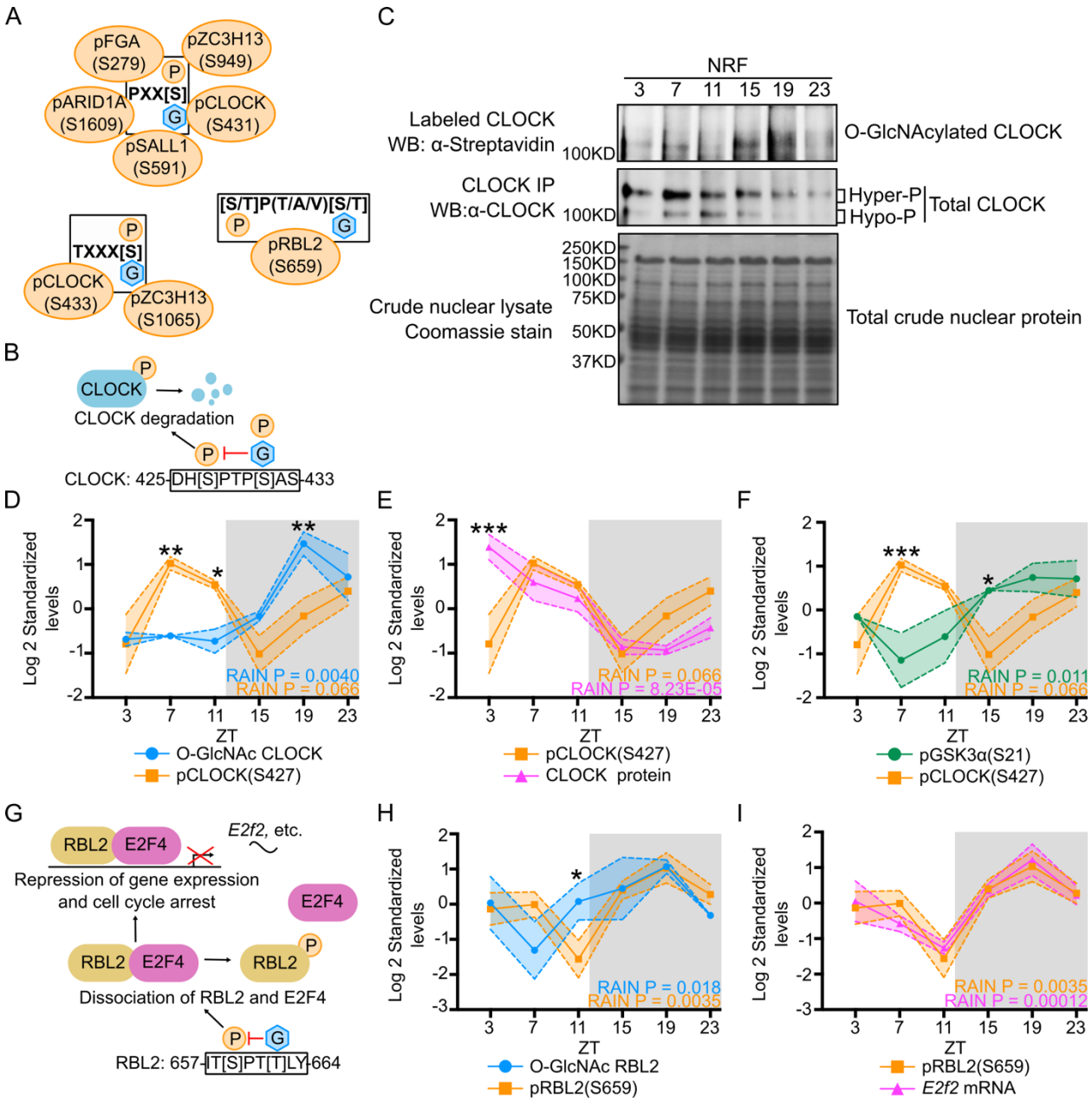

Fig 5 O-GlcNAcylation interacts with phosphorylation to regulate rhythmic function of CLOCK and RBL2. (A) Schematics showing different types of O-GlcNAcylation and phosphorylation interplay motifs. Phosphorylation sites located within these motifs are indicated in the bubbles around each motif. O-GlcNAcylation either targets the same sites or approximal sites as indicated in each motif. **(B)** Model showing competition between O-GlcNAcylation and phosphorylation at CLOCK(S431) to inhibit CLOCK(S427) phosphorylation. Since S431 and S427 belong to a phospho-degron, O-GlcNAcylation at S431 could stabilize CLOCK by reducing phosphorylation at both sites. **(C)** Representative blot showing the daily rhythms of CLOCK O-

GlcNAcylation (Top panel) and protein level (Middle panel). Total nuclear proteins were stained with Coomassie blue (Bottom panel) and used for normalization. Mice were fed at natural night feeding time (NRF). **(D-F)** Graphs comparing the daily patterns of CLOCK global O-GlcNAcylation vs CLK(S427) phosphorylation levels **(D)**, CLOCK(S427) phosphorylation vs CLOCK protein levels **(E)**, and GSK3α(S21) vs CLOCK(S427) phosphorylation levels **(F)**. **(G)** Model showing the inhibition of RBL2 S659 phosphorylation by O-GlcNAcylation. Phosphorylation of RBL2 S659 can promote the dissociation between RBL2 and E2F4 and thereby remove the inhibitory effect of RBL2-E2F4 complex on target genes. *E2f2* is one of the target genes critical for cell cycle progression. **(H and I)** Graphs to compare the daily rhythms between RBL2 O-GlcNAcylation vs S659 phosphorylation levels **(H)**, and RBL2(S659) phosphorylation vs *E2f2* mRNA expression levels **(I)**. The gray shading illustrates the dark phase of a day-night cycle. Data are presented as mean ± SEM (n = 2 or 3), and the shading area around the curves represents SEM. *$p < 0.05$, **$p < 0.0021$, ***$p < 0.0002$, two-way ANOVA with post-hoc Fisher's LSD tests.

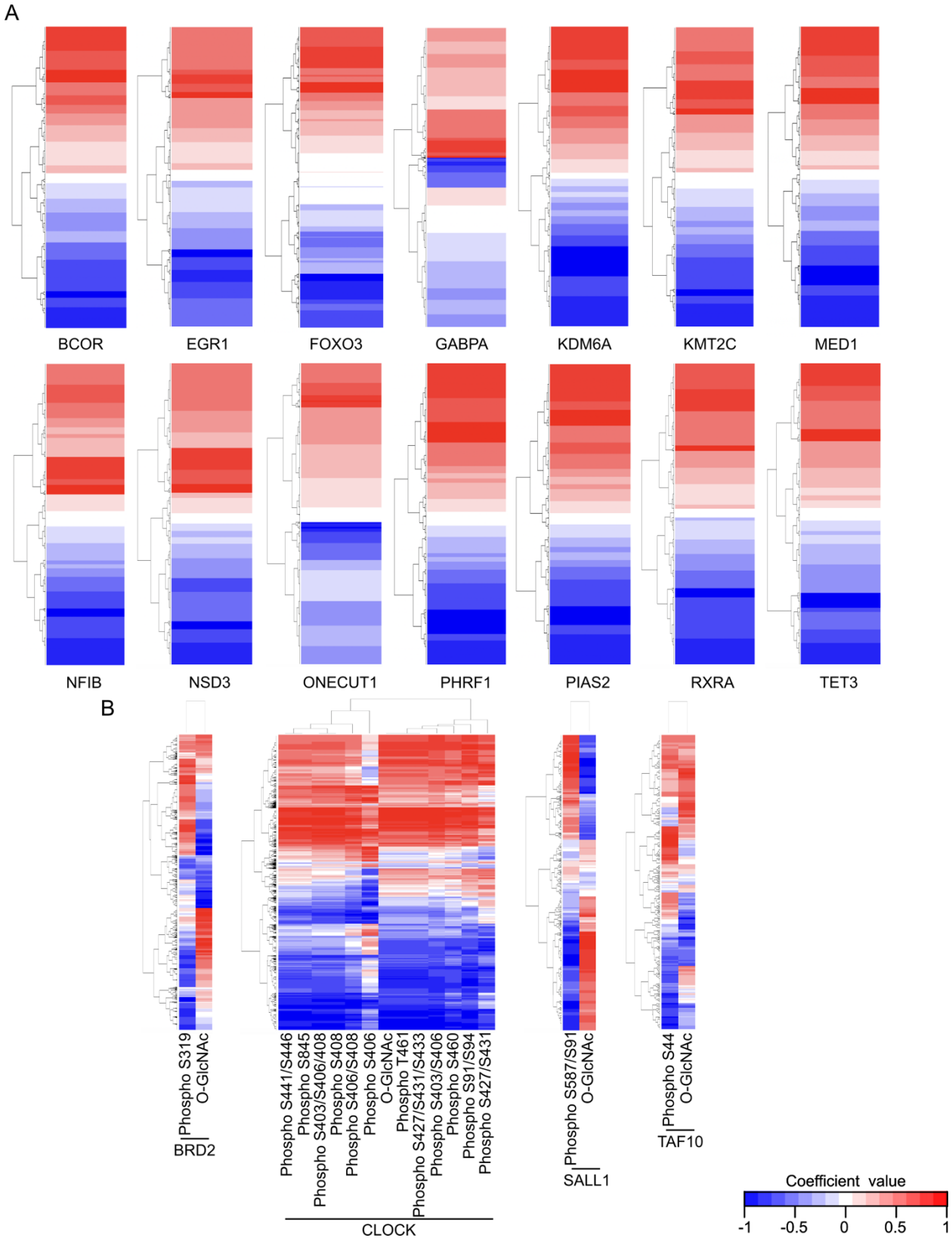
A
BCOR
EGR1
FOXO3
GABPA
KDM6A
KMT2C
MED1
NFIB
NSD3
ONECUT1
PHRF1
PIAS2
RXRA
TET3
B
Phospho S319
O-GlcNAc
BRD2
Phospho S441/S446
Phospho S845
Phospho S403/S406/408
Phospho S408
Phospho S406/S408
Phospho S406
O-GlcNAc
Phospho T461
Phospho S427/S431/S433
Phospho S403/S406
Phospho S460
Phospho S91/S94
Phospho S427/S431
CLOCK
Phospho S587/S91
O-GlcNAc
SALL1
Phospho S44
O-GlcNAc
TAF10
Coefficient value
-1
-0.5
0
0.5
1

Fig 6. Correlation of target gene expression with O-GlcNAcylation and G-P interactive phosphorylation rhythms on transcription factors. Spearman correlation analysis showing the correlation between rhythmic target gene transcription and rhythmic O-GlcNAcylation of transcription factors (**A**) and between rhythmic target gene transcription and rhythmic O-GlcNAcylation and G-P interactive phosphopeptides of transcription factors (**B**). The color of the heatmap represents coefficient values.

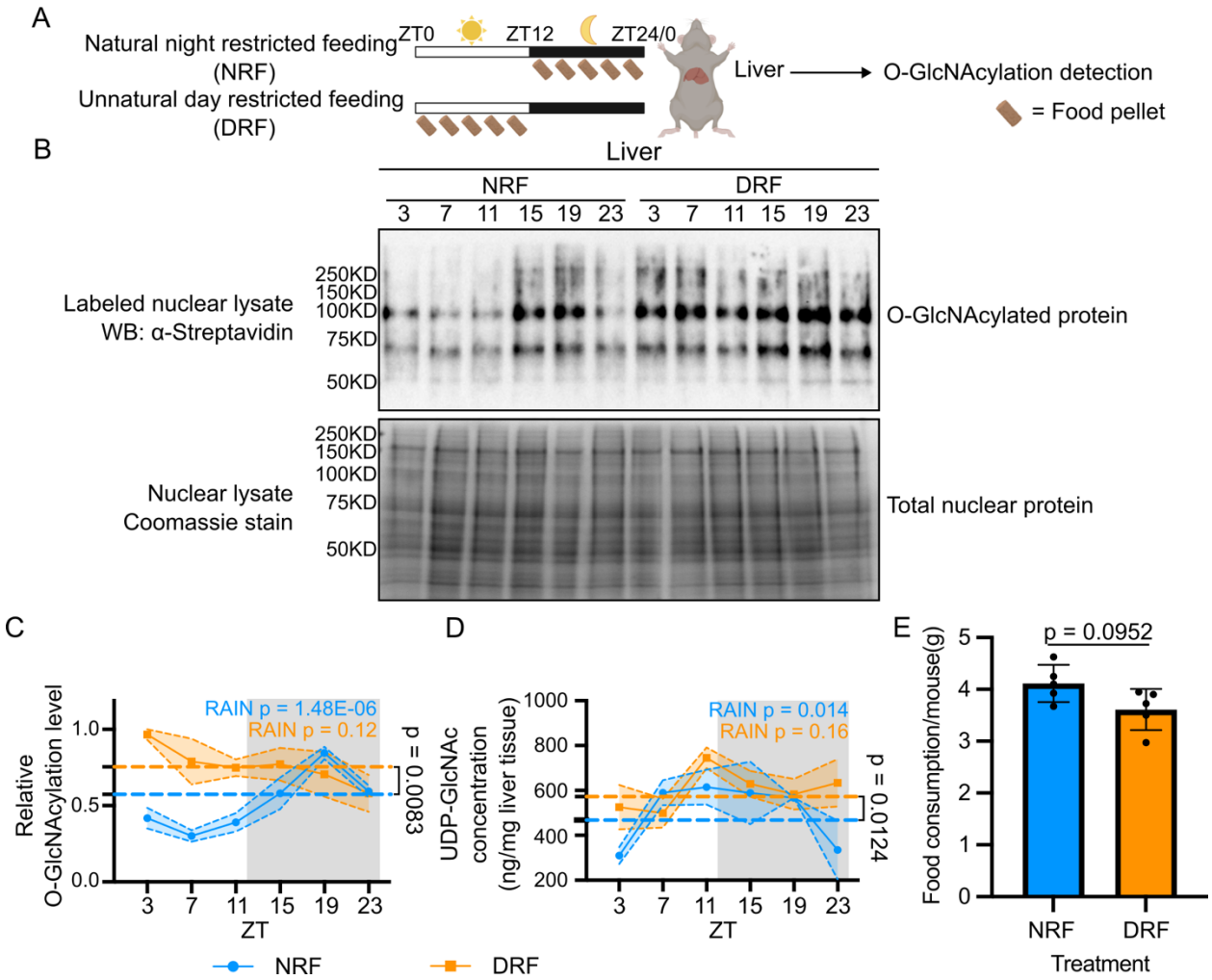

Fig 7. Time of food consumption affects daily protein O-GlcNAcylation rhythm in mouse liver. (A) Schematics showing the study design. 8-week-old C57BL/6 male mice were split into two groups, natural night restricted feeding (NRF) and unnatural day restricted feeding (DRF). The natural feeding group was only fed during the dark phase (ZT12-24), while the unnatural feeding group was only fed during the light phase (ZT0-12). After 3 weeks of treatment, mouse

livers were collected at 4h intervals over one day, and global O-GlcNAcylation of liver nuclear proteins were detected. **(B)** Representative blot showing the daily rhythm of nuclear protein O-GlcNAcylation in liver samples from the NRF vs DRF mice (Top panel). Total nuclear proteins were stained with Coomassie blue (Bottom panel) and used for normalization. **(C)** Quantification of protein O-GlcNAcylation signals in **(B)** (n = 3). The α-streptavidin signal of the entire lane was quantified. **(D)** Daily rhythm of UDP-GlcNAc were quantified using targeted metabolomics (n = 3). The dashed lines represent the median levels of O-GlcNAcylation **(C)** or UDP-GlcNAc **(D)** in NRF and DRF groups, and Student's t test was used to assess significant difference. The gray shading illustrates the dark phase of a day-night cycle. Data are presented as mean ± SEM, and the shading area around the curves represents SEM. **(E)** Food consumption of NRF and DRF mice over a 24-hr period (n=5). P=0.0952, Mann-Whitney test.

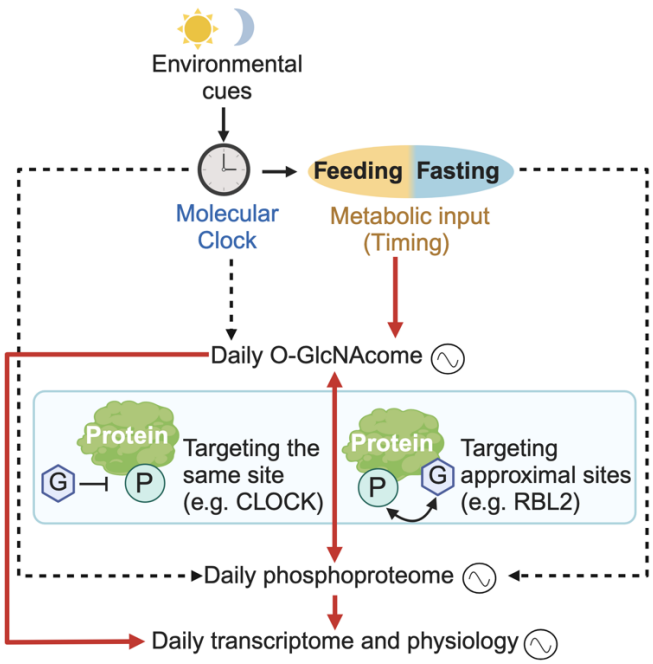

Fig 8. Model describing how daily rhythmic O-GlcNAcome integrates environmental and metabolic signals to regulate transcriptomic and physiological rhythms. Environmental cues signaling through the molecular clock and metabolic cues from feeding-fasting cycles regulate daily rhythms in the O-GlcNAcome. Rhythmic O-GlcNAcylation can directly shape daily rhythmicity in transcriptome and physiology. In addition, rhythmic O-GlcNAcylation can also interact with rhythmic phosphorylation. Different forms of crosstalk between O-GlcNAcome and phosphoproteome are shown in the middle box. The red solid arrows indicate the regulations

described in this study, while the dashed arrow indicates regulations discovered by previous studies [30,57,58]. Figure created using BioRender.com.

Supporting information

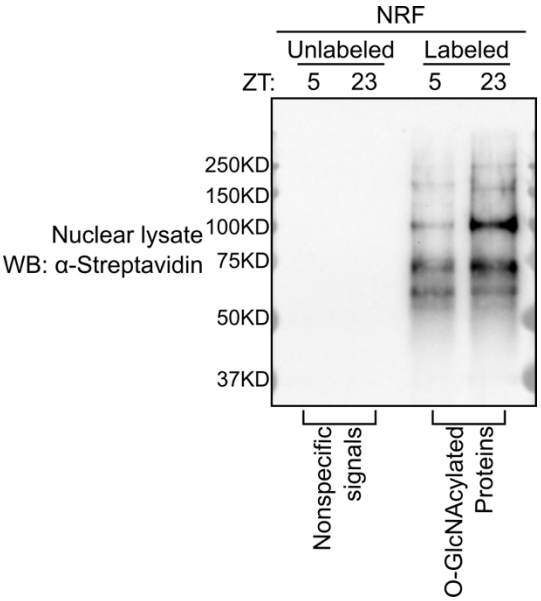

S1 Fig. Validation of chemoenzymatic labeling method for O-GlcNAcylation detection in mouse liver tissues. Two samples for the NRF group were chosen to show time-specific difference of liver nuclear O-GlcNAcylation (Lanes 3-4). Lanes 1-2 show the unlabeled samples processed in parallel with the labeled samples in Lanes 3-4. GalT1 enzyme was excluded during the processing of unlabeled samples.

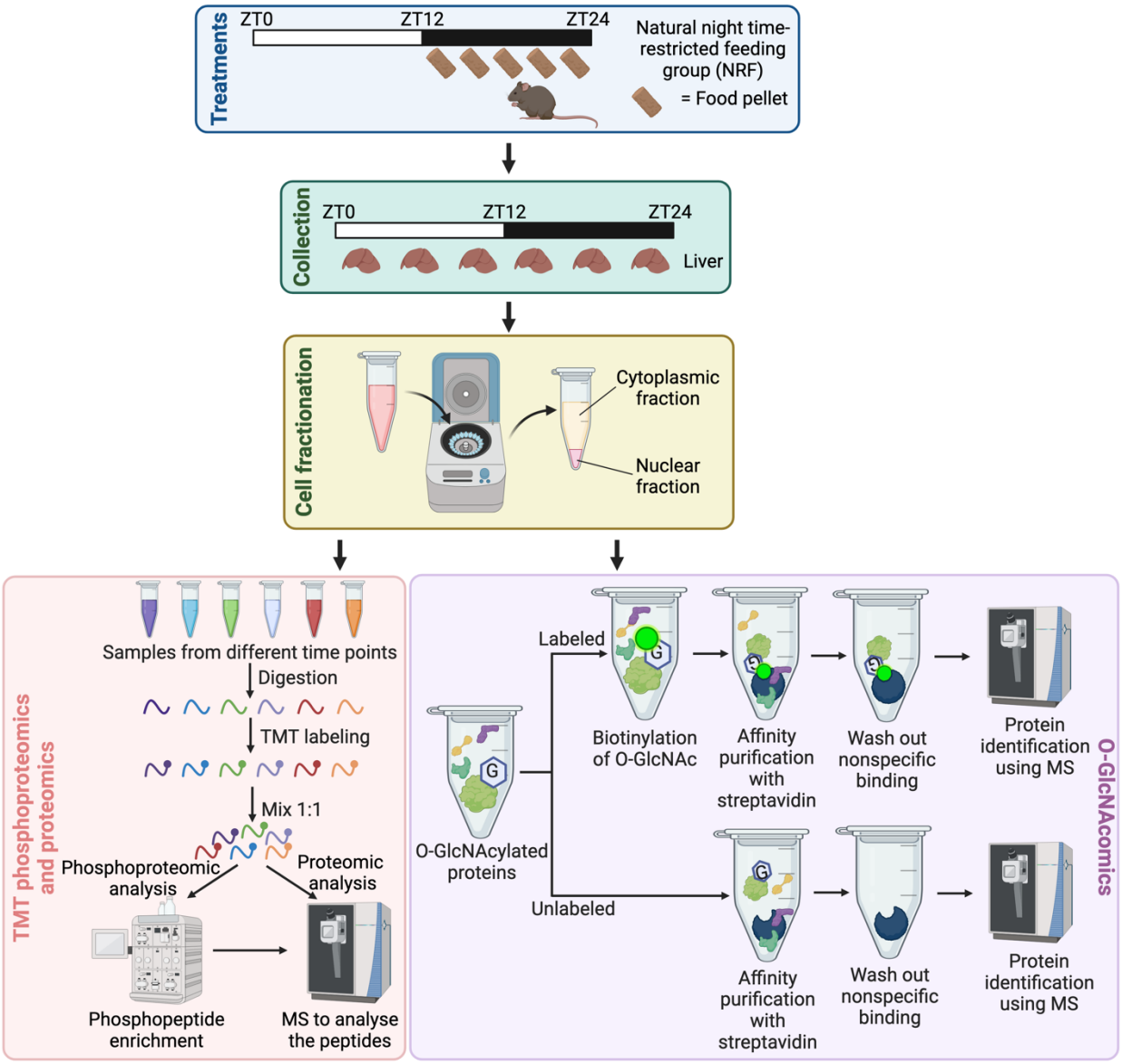

S2 Fig. Study design for O-GlcNAcomics and TMT phosphoproteomics analysis. Flow chart illustrating the design of the proteomics experiments using mice subjected to night time-restricted feeding (NRF). Liver samples were collected at 6 time-points over a 24h day-night cycle. Nuclear extracts were used for site-specific TMT phosphoproteomics and global O-GlcNAcomics. During the process of TMT phosphoproteomics, samples were first labeled with TMT tags, and the majority of the samples were used for enrichment of phospho-peptide followed by MS analysis. A small portion of TMT-labled samples were used for proteomic analysis, where samples were directly subjected to MS analysis without enrichment. The protein levels obtained from proteomic analysis were used for normalizing phosphoproteomic and O-GlcNAcomic datasets. During the process of O-GlcNAcomics, the O-GlcNAcylation groups on proteins were biontinylated using the chemoenzymatic labeling. The O-GlcNAcylated proteins were purified using streptavidin beads followed by MS analysis. Unlabeled samples were processed in parallel, where the biotin was not attached to the O-GlcNAcylated proteins. Unlabeled samples were used for identifying

the *bona fide* O-GlcNAcylated proteins during bioinformatic analysis. G in the hexagons represent the O-GlcNAc groups on proteins.

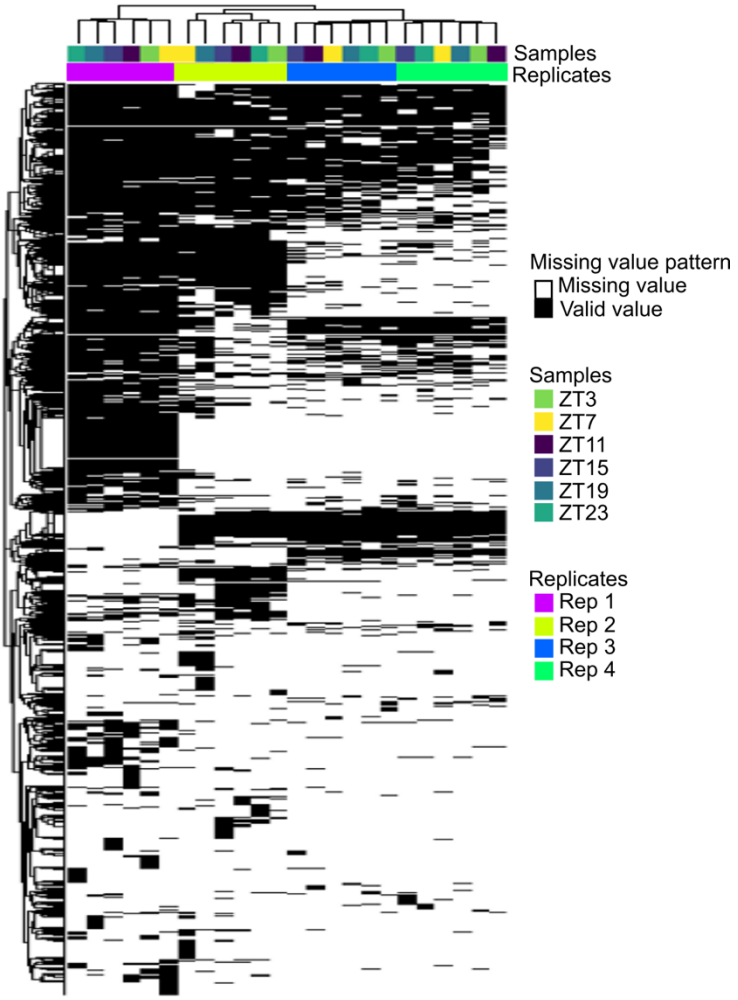

S3 Fig. Batch effects for O-GlcNAcome dataset. In the heatmap, if O-GlcNAc proteins were detected in the O-GlcNAcomic analysis (presence or absence), it is represented as black (valid values) in the corresponding samples. Otherwise, it would be represented as white (missing values). Biological replicates 1 and 2 were analyzed in one mass spectrometry run, while biological replicates 3 and 4 were analyzed in a separate mass spectrometry run. There are more commonly detected proteins in biological replicates 1 and 2, while the same is true for biological replicates 3 and 4. Therefore, replicates 1 and 2 are classified as batch 1, and replicates 3 and 4 as batch 2 for the O-GlcNAcomic bioinformatic analysis (SAINT to compare labeled and unlabeled samples and RAIN rhythmic analysis).

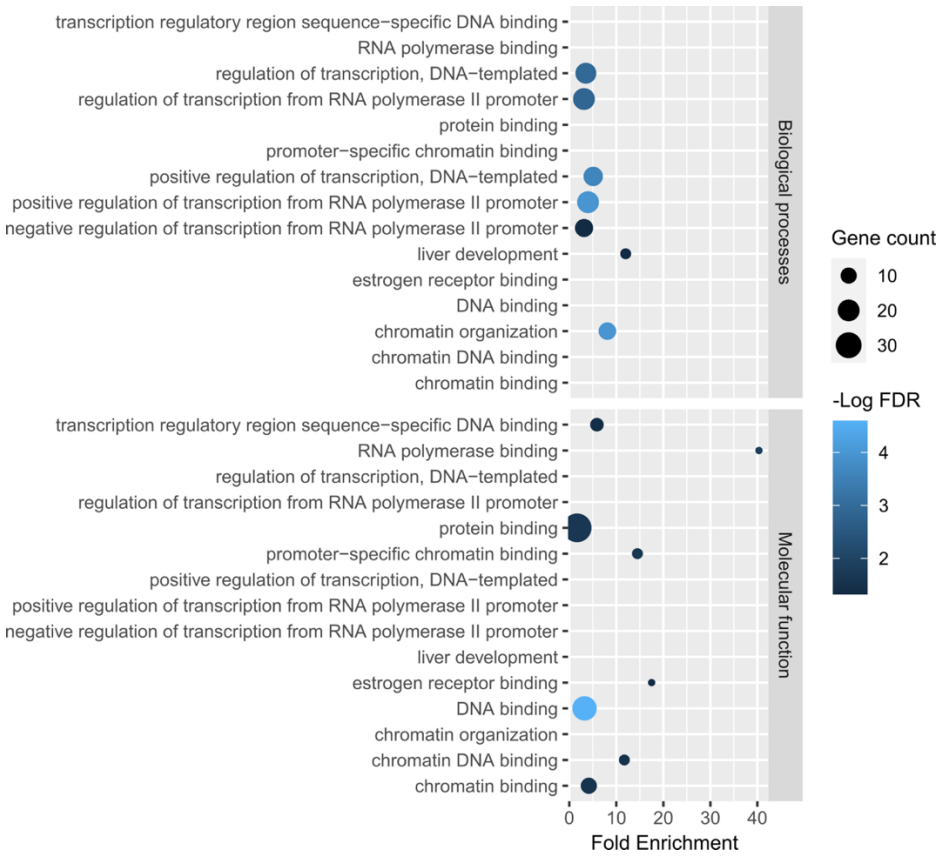

S4 Fig. Functional enrichment analysis of rhythmic O-GlcNAcome in mouse liver nuclei. Rhythmically O-GlcNAcylated proteins were fed into the Database for Annotation, Visualization and Integrated Discovery (DAVID) for enrichment of GO terms. The enriched biological processes and molecular functions were illustrated using bubble plots. The color of the bubbles indicates the -log10 false discovery rate (FDR), while the size of the bubbles indicates the number of genes in each enriched term.

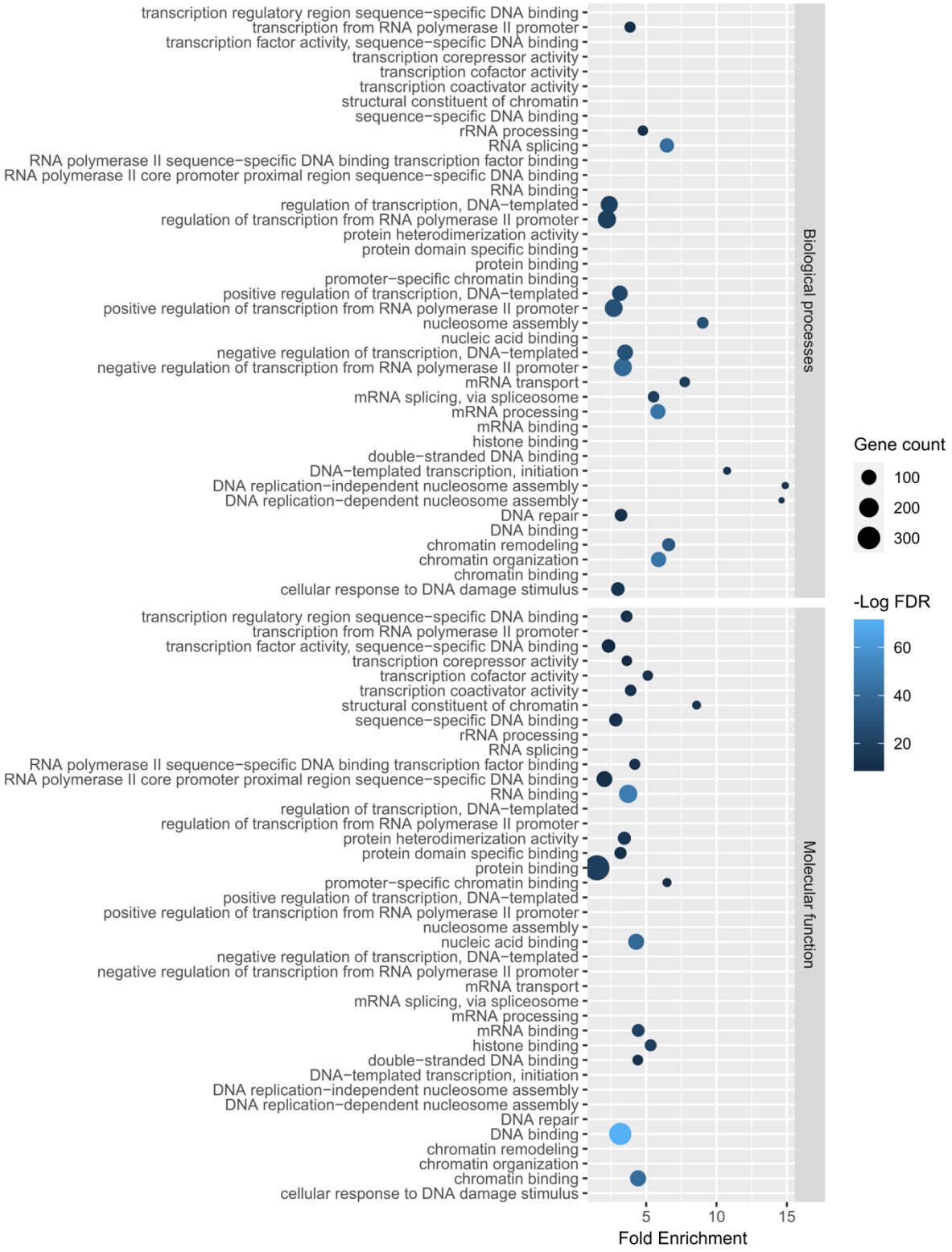

S5 Fig. Functional enrichment analysis of rhythmic phosphoproteome in mouse liver nuclei. Rhythmically phosphorylated proteins were fed into the DAVID database for enrichment of GO terms. The enriched biological processes and molecular functions were illustrated using bubble

plots. The color of the bubbles indicates the -log10 false discovery rate (FDR), while the size of the bubbles indicates the number of genes in each enriched term.

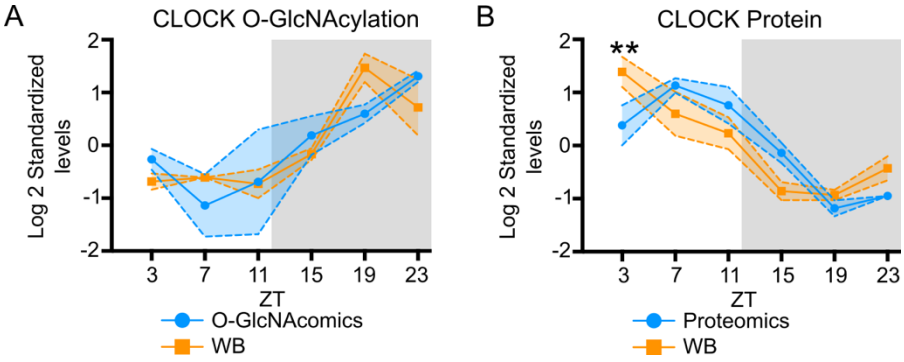

S6 Fig. Comparison of CLOCK detection using mass spectrometry and western blot. (A-B) Comparison of CLOCK O-GlcNAcylation **(A)** and protein level **(B)** detected by mass spectrometry and western blots. The gray shading illustrates the dark phase of a day-night cycle. Data are presented as mean ± SEM, and the shading area around the curves represents SEM (n= 2 or 3). **$p < 0.0021$, two-way ANOVA with post-hoc Fisher's LSD tests.

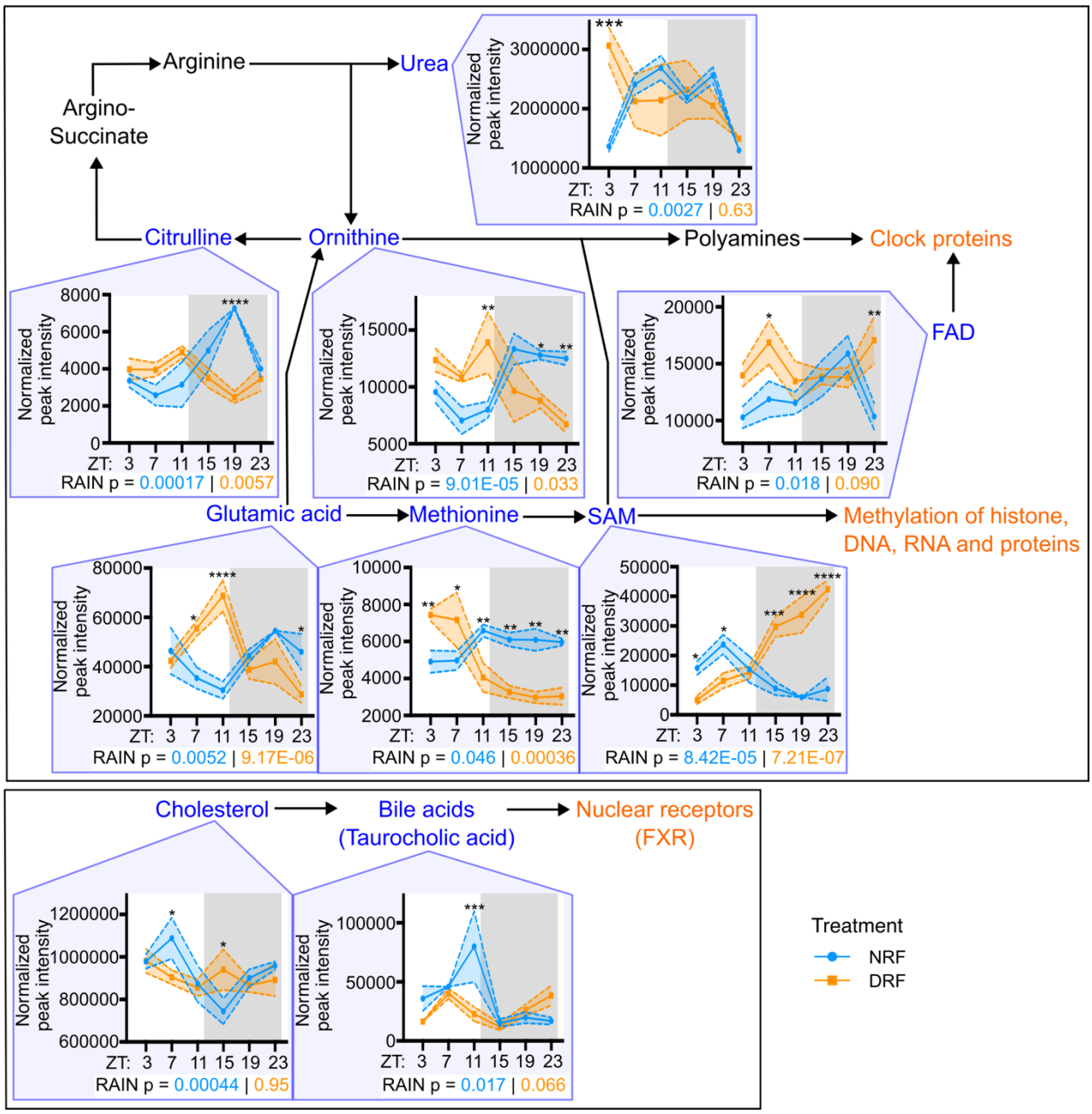

S7 Fig. Metabolic pathways other than the Hexosamine Biosynthetic Pathway (HBP) that can be involved in the regulation of gene expression. Since many metabolites were shown to regulate the function of clock proteins and other cellular proteins (Reviewed in Panda [1]), we searched for metabolites that are rhythmic under natural night restricted feeding (NRF) condition in our metabolomic dataset, and evaluated the impact of timing of food consumption on these rhythms by comparing their rhythmicity to that under unnatural day restricted feeding (DRF) condition. The gray shading illustrates the dark phase of a day-night cycle. Data are presented as mean ± SEM, and the shading area around the curves represents SEM (n= 3). p values from RAIN analysis for NRF (blue) and DRF (orange) are presented under each graph. *$p < 0.05$, **$p < 0.0021$, ***$p < 0.0002$, ****$p < 0.0001$, two-way ANOVA with post-hoc Fisher's LSD tests.

Table S1. Comparison between our study and published liver phosphoproteome datasets.

Reference	Number of phospho-peptides	Number of phospho-proteins	Number of oscillating phospho-peptides (Percentage)	Number of oscillating phospho-proteins (Percentage)	Circadian kinases	Normalize to protein level	Label method	TRF	LD vs DD	Cell fraction	Time points X days	Replicate number (total sample number)
This study	19593	3272	2376 (12.12%)	993 (30.35%)	AKT, GSK, S6K, MAPK, PKA, CDK, NLK, PAK, DAPK3, STK, TLK	Yes	TMT	Yes (3 weeks)	LD	Nucleus	6 time points X 1 day	3 (18)
Robles et al. [2]	7896	2672	2123 (26.89%)	1088 (40.71%)	ERK, MEK, RSK, JNK, AKT, mTOR, p70S6K Kinase, CK1δ	No	No	No	DD	Whole cell	8 time points X 2 days	4 (64)
Huang et al. [3]	NA	2639	NA	1668 (63.21%)	NA	No	No	Yes (1 week)	LD	Whole cell	6 time points X 2 day	4 (48)
Wang et al. [4]	9465	1657	NA	89 (5.37%)	NA	No	No	No	LD	Whole cell	8 time points X 2 days	1 (Pooled 3 mice) (16)
Wang et al. [5]	1448	NA	154 (10.64%)	113	GSK3α, GSK3β,CK1α, CK1δ, CDK1, CDK4, CDK6	No	SILAC	Yes (4 days)	LD	Nucleus	8 time points X 2 days	1 (16)

Table S2. Known functions of rhythmic phosphorylation sites that are identified in protein complexes.

Gene name	Uniprot ID	Phosphosite	Kinase	Function	Reference
Hdac1	O09106	S421, S423	CK2	Phosphorylation of S421 and S423 promotes the deacetylase activity and complex formation of HDAC1	[6]
Trim28	Q62318	S473	CHK1, CHK2, PKCδ, p38 MAPK	S473 phosphorylation regulates the ability of TRIM28 to induce cell cycle, promote DNA repair, induce cytokine production, inhibit aggresome formation, reinstate heterochromatin after DNA replication, and limit mitochondrial fusion	[7–16]
Mecp2	Q9Z2D6	S216	HIPK1, HIPK2	Phosphorylation of S216 stabilizes MECP2	[17]
		S80	HIPK2	Phosphorylation on S80 increases MeCP2 binding to chromatin and target gene promoters	[18–21]
Clock	O08785	T461	CDK5	T461 phosphorylation reduces stability and promotes nuclear translocation of CLOCK	[22]
		S431	NA	Phosphorylation of S431 primes the phosphorylation of S427	[23]
		S427	GSK3β	Phosphorylation of S427 leads to CLOCK degradation	[23]
		S845	AKT	Phosphorylation of S845 inhibits its nuclear translocation and affects circadian gene expression	[24]
Smc3	Q9CW03	S1083	ATM/ATR	Phosphorylation of S1083 induces SMC3 binding at cohesion sites in response to DNA damage	[25]
Rbl2	Q64700	S410, S659	NA	Phosphorylation of S410 and S659 (S413 and S662 in human homolog) promotes the dissociation between RBL2 and E2F4, and relieves repression of E2F4 target gene expression.	[26]
		S935	AKT	Phosphorylation of S935 (S941 in human homolog) decreases RBL2 protein stability	[27]
Sfpq	Q8VIJ6	T679	GSK3	Phosphorylation of T679 (T687 in human homolog) increases the interaction between SFPQ and TRAP150, which inhibits the binding of SFPQ pre-mRNA and thus affects its RNA splicing activity.	[28]

Table S3. The domains containing rhythmic phosphosites with unknown function and domains nearby (only phosphosites identified in protein complexes are included).

Gene name	Uniprot ID	Phosphosite	Nearby domains* (amino acid number of the domains)	Distance from nearby domain
Zc3h13	E9Q784	S64	ZF-CCCH domain (aa38-63)	+1
Ptbp2	Q91Z31	S308	RNA recognition motif (aa309-434)	-1
Hnrnpf	Q9Z2X1	S193	RNA recognition motif (aa113-182)	+11
Hnrnpm	Q9D0E1	S636	RNA recognition motif (aa654-722)	-18
Rbl2	Q64700	Y632	RB A (aa414-606)	+26
		S959	RB B (aa831-1012)	0
		S935	RB B (aa831-1012)	0
		S937	RB B (aa831-1012)	0
Zfpm1	O35615	S925	zf-met (963-983)	-38
		S927	zf-met (963-983)	-36
Gatad2b	Q8VHR5	S123	p66 CC (158-201)	-35
		S487	GATA (421-455)	+32
		T121	p66 CC (158-201)	-37
		S136	p66 CC (158-201)	-22
Mta2	Q9R190	S435	GATA (367-404) and MTA R1 (447-524)	+31 and -12
Mbd3	Q9Z2D8	Y83	MBDa (79-148)	0
Sin3a	Q60520	S939	Sin3a C (887-1187)	0
Mecp2	Q9Z2D6	T64	MBD (91-162)	-27
Smarca4	Q3TKT4	S1388	SnAC (1289-1356)	+32
		S1536	Bromodomain (1429-1517)	+19
		S1541	Bromodomain (1429-1517)	+24
		S1389	Bromodomain (1429-1517) and SnAC (1289-1356)	-40 and +33
Med7	Q9CZB6	S195	Med7 (7-164)	+31
Clock	O08785	S91	HLH (35-85)	+6
		S94	HLH (35-85)	+9
		S403	PAS 11 (273-380)	+23
		S406	PAS 11 (273-380)	+26
		S408	PAS 11 (273-380)	+28
Ncl	P09405	S605	RRM1 (574-641)	0
		S462	RRM1 (395-460)	+2
		T307	RRM1 (309-377)	-2
		S563	RRM1 (489-555) and RRM1 (571-638)	+8 and -8
		S616	RRM1 (574-641)	0
Smc1a	Q9CU62	S649	SMC hinge SMC N (512-629)	0

S1 File. Targeted metabolomics of NRF and DRF mouse liver for hexosamine biosynthetic pathway (HBP). Peak intensities of metabolites detected using GC-MS and calculated concentration of HBP metabolites.

S2 File. Nuclear O-GlcNAcome of NRF mouse liver. (Tab 1) Normalized peptide counts for nuclear O-GlcNAcome. (Tab 2) Results of rhythmicity analysis for O-GlcNAcome using RAIN.

S3 File. Nuclear proteome of NRF mouse liver. Peptide counts and rhythmicity analysis of nuclear proteome.

S4 File. Protein complex analysis for rhythmic O-GlcNAcome. List of protein complexes that contain rhythmically O-GlcNAcylated proteins, with the rhythmic subunits and the function of protein complexes indicated.

S5 File. Nuclear phosphoproteome of NRF mouse liver. Normalized peptide counts and rhythmicity analysis of nuclear phosphoproteome.

S6 File. Rhythmic kinases detected in proteomic, phosphoproteomic, and O-GlcNAcomic datasets. (Tab 1-3) Lists of kinases and their rhythmicity analysis from our proteomic, phosphoproteomics and O-GlcNAcomic datasets, respectively.

S7 File. Protein complex analysis for rhythmic phosphoproteome. List of protein complexes that contain rhythmically phosphorylated proteins, with the rhythmic subunits and the function of protein complexes indicated.

S8 File. Rhythmic phosphosites that belong to G-P interplay motifs. List of proteins and their phosphosites identified by G-P interplay motif analysis. The G-P interplay motifs for each phosphosites are indicated.

Supplementary references

1. Panda S. Circadian physiology of metabolism. Science. 2016;354: 1008–1015. doi:10.1126/science.aah4967

2. Robles MS, Humphrey SJ, Mann M. Phosphorylation Is a Central Mechanism for Circadian Control of Metabolism and Physiology. Cell Metabolism. 2017;25: 118–127. doi:10.1016/j.cmet.2016.10.004

3. Huang R, Chen J, Zhou M, Xin H, Lam SM, Jiang X, et al. Multi-omics profiling reveals rhythmic liver function shaped by meal timing. Nat Commun. 2023;14: 6086. doi:10.1038/s41467-023-41759-9

4. Wang Y, Song L, Liu M, Ge R, Zhou Q, Liu W, et al. A proteomics landscape of circadian clock in mouse liver. Nat Commun. 2018;9: 1553. doi:10.1038/s41467-018-03898-2

5. Wang J, Mauvoisin D, Martin E, Atger F, Galindo AN, Dayon L, et al. Nuclear Proteomics Uncovers Diurnal Regulatory Landscapes in Mouse Liver. Cell Metabolism. 2017;25: 102–117. doi:10.1016/j.cmet.2016.10.003

6. Pflum MK, Tong JK, Lane WS, Schreiber SL. Histone deacetylase 1 phosphorylation promotes enzymatic activity and complex formation. J Biol Chem. 2001;276: 47733–47741. doi:10.1074/jbc.M105590200

7. Bolderson E, Savage KI, Mahen R, Pisupati V, Graham ME, Richard DJ, et al. Kruppel-associated Box (KRAB)-associated co-repressor (KAP-1) Ser-473 phosphorylation regulates heterochromatin protein 1β (HP1-β) mobilization and DNA repair in heterochromatin. J Biol Chem. 2012;287: 28122–28131. doi:10.1074/jbc.M112.368381

8. Hu C, Zhang S, Gao X, Gao X, Xu X, Lv Y, et al. Roles of Kruppel-associated Box (KRAB)-associated Co-repressor KAP1 Ser-473 Phosphorylation in DNA Damage Response. J Biol Chem. 2012;287: 18937–18952. doi:10.1074/jbc.M111.313262

9. Blasius M, Forment JV, Thakkar N, Wagner SA, Choudhary C, Jackson SP. A phospho-proteomic screen identifies substrates of the checkpoint kinase Chk1. Genome Biol. 2011;12: R78. doi:10.1186/gb-2011-12-8-r78

10. Chang C-W, Chou H-Y, Lin Y-S, Huang K-H, Chang C-J, Hsu T-C, et al. Phosphorylation at Ser473 regulates heterochromatin protein 1 binding and corepressor function of TIF1beta/KAP1. BMC Mol Biol. 2008;9: 61. doi:10.1186/1471-2199-9-61

11. Jang SM, Kauzlaric A, Quivy J-P, Pontis J, Rauwel B, Coluccio A, et al. KAP1 facilitates reinstatement of heterochromatin after DNA replication. Nucleic Acids Res. 2018;46: 8788–8802. doi:10.1093/nar/gky580

12. Cheng C-T, Kuo C-Y, Ouyang C, Li C-F, Chung Y, Chan DC, et al. Metabolic Stress-Induced Phosphorylation of KAP1 Ser473 Blocks Mitochondrial Fusion in Breast Cancer Cells. Cancer Res. 2016;76: 5006–5018. doi:10.1158/0008-5472.CAN-15-2921

13. Shen LT-W, Chou H-YE, Kato M. TIF1β is phosphorylated at serine 473 in colorectal tumor cells through p38 mitogen-activated protein kinase as an oxidative defense mechanism. Biochem Biophys Res Commun. 2017;492: 310–315. doi:10.1016/j.bbrc.2017.08.117

14. White D, Rafalska-Metcalf IU, Ivanov AV, Corsinotti A, Peng H, Lee S-C, et al. The ATM substrate KAP1 controls DNA repair in heterochromatin: regulation by HP1 proteins and serine 473/824 phosphorylation. Mol Cancer Res. 2012;10: 401–414. doi:10.1158/1541-7786.MCR-11-0134

15. Zu R, Yu Z, Zhao J, Lu X, Liang W, Sun L, et al. Quantitative analysis of phosphoproteome in necroptosis reveals a role of TRIM28 phosphorylation in promoting necroptosis-induced cytokine production. Cell Death Dis. 2021;12: 994. doi:10.1038/s41419-021-04290-7

16. Chang J, Hwang HJ, Kim B, Choi Y-G, Park J, Park Y, et al. TRIM28 functions as a negative regulator of aggresome formation. Autophagy. 2021;17: 4231–4248. doi:10.1080/15548627.2021.1909835

17. Lombardi LM, Zaghlula M, Sztainberg Y, Baker SA, Klisch TJ, Tang AA, et al. An RNA interference screen identifies druggable regulators of MeCP2 stability. Sci Transl Med. 2017;9: eaaf7588. doi:10.1126/scitranslmed.aaf7588

83 18. Schmidt A, Frei J, Poetsch A, Chittka A, Zhang H, Aßmann C, et al. MeCP2 heterochromatin
84 organization is modulated by arginine methylation and serine phosphorylation. Front Cell Dev
85 Biol. 2022;10: 941493. doi:10.3389/fcell.2022.941493

86 19. Tao J, Hu K, Chang Q, Wu H, Sherman NE, Martinowich K, et al. Phosphorylation of MeCP2 at
87 Serine 80 regulates its chromatin association and neurological function. Proc Natl Acad Sci U S A.
88 2009;106: 4882–4887. doi:10.1073/pnas.0811648106

89 20. Moran-Salvador E, Garcia-Macia M, Sivaharan A, Sabater L, Zaki MYW, Oakley F, et al.
90 Fibrogenic Activity of MECP2 Is Regulated by Phosphorylation in Hepatic Stellate Cells.
91 Gastroenterology. 2019;157: 1398-1412.e9. doi:10.1053/j.gastro.2019.07.029

92 21. Bracaglia G, Conca B, Bergo A, Rusconi L, Zhou Z, Greenberg ME, et al. Methyl-CpG-binding
93 protein 2 is phosphorylated by homeodomain-interacting protein kinase 2 and contributes to
94 apoptosis. EMBO Rep. 2009;10: 1327–1333. doi:10.1038/embor.2009.217

95 22. Kwak Y, Jeong J, Lee S, Park Y-U, Lee S-A, Han D-H, et al. Cyclin-dependent kinase 5 (Cdk5)
96 regulates the function of CLOCK protein by direct phosphorylation. J Biol Chem. 2013;288:
97 36878–36889. doi:10.1074/jbc.M113.494856

98 23. Spengler ML, Kuropatwinski KK, Schumer M, Antoch MP. A serine cluster mediates BMAL1-
99 dependent CLOCK phosphorylation and degradation. Cell Cycle. 2009;8: 4138–4146.
100 doi:10.4161/cc.8.24.10273

101 24. Luciano AK, Zhou W, Santana JM, Kyriakides C, Velazquez H, Sessa WC. CLOCK
102 phosphorylation by AKT regulates its nuclear accumulation and circadian gene expression in
103 peripheral tissues. J Biol Chem. 2018;293: 9126–9136. doi:10.1074/jbc.RA117.000773

104 25. Kim B-J, Li Y, Zhang J, Xi Y, Li Y, Yang T, et al. Genome-wide reinforcement of cohesin binding
105 at pre-existing cohesin sites in response to ionizing radiation in human cells. J Biol Chem.
106 2010;285: 22784–22792. doi:10.1074/jbc.M110.134577

107 26. Farkas T, Hansen K, Holm K, Lukas J, Bartek J. Distinct phosphorylation events regulate p130- and
108 p107-mediated repression of E2F-4. J Biol Chem. 2002;277: 26741–26752.
109 doi:10.1074/jbc.M200381200

110 27. Pentimalli F, Forte IM, Esposito L, Indovina P, Iannuzzi CA, Alfano L, et al. RBL2/p130 is a direct
111 AKT target and is required to induce apoptosis upon AKT inhibition in lung cancer and
112 mesothelioma cell lines. Oncogene. 2018;37: 3657–3671. doi:10.1038/s41388-018-0214-3

113 28. Heyd F, Lynch KW. Phosphorylation-dependent regulation of PSF by GSK3 controls CD45
114 alternative splicing. Mol Cell. 2010;40: 126–137. doi:10.1016/j.molcel.2010.09.013

115